Original Research Communication

ACUTE LIVER INJURY INDUCES NUCLEOCYTOPLASMIC REDISTRIBUTION OF HEPATIC METHIONINE METABOLISM ENZYMES

Miguel Delgado[1], Francisco Garrido[1], Juliana Pérez-Miguelsanz[1,2], María Pacheco[1], Teresa Partearroyo[3], Dolores Pérez-Sala[4] and María A. Pajares[1,5*]

[1]Instituto de Investigaciones Biomédicas "Alberto Sols" (CSIC-UAM), Arturo Duperier 4, 28029 Madrid, Spain. [2]Departamento de Anatomía y Embriología Humana I, Facultad de Medicina, Universidad Complutense de Madrid, Plaza de Ramón y Cajal s/n, 28040 Madrid, Spain. [3]Departamento de Ciencias Farmacéuticas y de la Salud, Facultad de Farmacia, Universidad CEU San Pablo, Boadilla del Monte, Madrid, Spain; [4]Centro de Investigaciones Biológicas (CSIC), Ramiro de Maeztu 9, 28040 Madrid, Spain. [5]Molecular Hepatology group, IdiPAZ, Pº de la Castellana 261, 28046 Madrid.

[*]To whom correspondence should be addressed: Instituto de Investigaciones Biomédicas Alberto Sols (CSIC-UAM), Arturo Duperier 4, 28029 Madrid, Spain (Phone: 34-915854414; FAX: 34-915854401; email: mapajares@iib.uam.es)

Running head: Liver injury and methionine metabolism

Word count: 5994

Reference numbers: 1-62 (1830 words)

Number of grayscale illustrations: 6

Number of color illustrations: 2 (online only)

ABSTRACT

Aims. The discovery of methionine metabolism enzymes in the cell nucleus, together with their association with key nuclear processes, suggested a putative relationship between alterations in their subcellular distribution and disease. *Results.* Using the rat model of D-galactosamine intoxication severe changes in hepatic steady-state mRNA levels were found; the largest decreases corresponded to enzymes exhibiting the highest expression in normal tissue. Cytoplasmic protein levels, activities and metabolite concentrations suffered more moderate changes following a similar trend. Interestingly, galactosamine-treatment induced hepatic nuclear accumulation of MATα1 and S-adenosylhomocysteine hydrolase tetramers, their active assemblies. In fact, galactosamine-treated livers showed enhanced nuclear methionine adenosyltransferase activity. Acetaminophen intoxication mimicked most galactosamine effects on hepatic MATα1, including accumulation of nuclear tetramers. H35 cells overexpressing tagged-MATα1 reproduced the subcellular distribution observed in liver, and the changes induced by galactosamine and acetaminophen that were also observed upon glutathione depletion by buthionine sulfoximine. The H35 nuclear accumulation of tagged-MATα1 induced by these agents correlated with decreased GSH/GSSG ratios and was prevented by N-acetylcysteine and glutathione ethyl ester. However, the changes in epigenetic modifications associated with tagged-MATα1 nuclear accumulation were only prevented by N-acetylcysteine in galactosamine-treated cells. *Innovation.* Cytoplasmic and nuclear changes in proteins regulating the methylation index follow opposite trends in acute liver injury, their nuclear accumulation showing potential as disease marker. *Conclusion.* Altogether these results demonstrate galactosamine- and acetaminophen-induced nuclear accumulation of methionine metabolism enzymes as active oligomers

and unveil the implication of redox-dependent mechanisms in the control of MATα1 subcellular distribution.

Keywords: Methionine adenosyltransferase, methylation index, epigenetic modifications, redox stress.

INTRODUCTION

Methionine is an essential amino acid that is mainly metabolized in the liver for protein and S-adenosylmethionine (AdoMet or SAM) synthesis. Reductions in AdoMet levels occur in a multitude of pathologies that include from cancer to acute liver failure (31, 37, 45). Three methyltransferases, among them glycine N-methyltransferase (GNMT), account for most of hepatic AdoMet consumption (32, 39). Methylations generate S-adenosylhomocysteine (AdoHcy), a potent inhibitor of many methyltransferases (9), the ratio AdoMet/AdoHcy (methylation index) determining the flow through these reactions (45). Methionine adenosyltransferases (MATs) are the only known enzymes that catalyze AdoMet synthesis using methionine and ATP in the first, and rate-limiting, reaction of the methionine cycle (45). AdoMet is used primarily for transmethylation reactions, but also by SAM radical proteins and after decarboxylation for polyamine biosynthesis (37, 45). S-adenosylhomocysteine hydrolase (SAHH) eliminates AdoHcy in a reversible reaction that favors its synthesis, unless homocysteine (Hcy) and adenosine are efficiently removed. Hcy can be remethylated to methionine by methionine synthase (MTR) or betaine homocysteine methyltransferase (BHMT), transported into the blood or enter the trans-sulfuration pathway (46). This last pathway connects methionine metabolism with cysteine and glutathione production, and hence with redox control.

Regulation of the methionine cycle is complicated by the existence of several isoenzymes (MAT I, II and III), the action exerted by several metabolites (AdoMet, AdoHcy) and the existence of homo- (i.e. MAT I and III, BHMT) and hetero-oligomers (MAT II) (45, 46). Different regulatory mechanisms contribute to determine the final outcome, involving: i) hormones, acting primarily at the transcriptional level (18); ii) metabolites that activate or inhibit several steps (e.g. AdoMet); iii) related metabolites

that modulate expression (e.g. methylthioadenosine), activity and oligomerization (e.g. glutathione and $NADP^+$)(12, 20, 44).

Many studies have been focused in analyzing the changes in expression, protein levels, and activity of MAT isoenzymes and their relationship with disease. Among them, rat models of galactosamine and CCl_4 intoxication in combination with biopsies of human cirrhotic livers showed decreased MAT activity and reductions in the MAT I (tetramer of α1) to MAT III (dimer of α1) activity ratio (7, 11). Additional studies demonstrated an expression switch from *MAT1A* (encoding α1 subunits) to *MAT2A* (encoding α2 subunits of MAT II) in hepatoma, resembling the fetal expression pattern (17). These changes decreased AdoMet concentrations, given the differences in V_{max} and methionine affinity of the isoenzymes (33, 45). The importance of AdoMet levels in liver disease was further demonstrated when mice exhibiting low (*MAT1A -/-)* and high (*GNMT -/-*) hepatic AdoMet levels were produced (30, 35). These mice developed HCC spontaneously, highlighting the necessity of a strict control of AdoMet homeostasis for normal liver function.

Recently, nuclear localization of some methionine cycle enzymes was reported. Nuclear MATα1 accumulation correlated with increased histone 3 K27 trimethylation (me3K27H3), an epigenetic modification related to gene repression (50). Nuclear MATα2 has been found acting as a MafK corepressor and interacting with histone 3 K9 and K4 dimethylating enzymes (26), and nuclear SAHH was related to efficient RNA cap methylation (49). However, the mechanisms regulating subcellular distribution of these proteins and its relationship with disease remain unknown. For this purpose, we have used models of acute liver injury as suitable experimental settings and found nuclear accumulation of methionine metabolism enzymes, together with the implication of a redox-dependent mechanism in the process. Altogether the results presented sustain

the novel paradigm of gene expression regulation through the nuclear shuttling of enzymes controlling the methylation index.

RESULTS

The rat model of D-galactosamine intoxication has been previously used to analyze changes in AdoMet production in hepatopathy, by measuring cytosolic MAT activity and AdoMet levels (7, 58). We reproduced this model in search of a putative link among disease and nucleocytoplasmic distribution of methionine cycle enzymes. No changes in liver weight, but striking differences in histology, between animals included in control and galactosamine groups were found (Supplementary Fig. S1). Control livers had normal appearance in hematoxylin/eosin staining, whereas galactosamine-treated animals showed intrasinusal lymphocytes, signs of steatosis and small focuses of necrosis. Galactosamine also induced a dramatic increase in serum transaminases, together with a significant reduction in hepatic AdoMet levels and total MAT activity (Supplementary Tables S1, S2). Analytical gel filtration chromatography (AGFC) showed a larger decline in MAT I than in MAT III activity, thus changing the MAT III/I ratio (Supplementary Fig. S2A, C, Table S1). Hence, the treatment was effective, livers showing the expected signs of hepatopathy and the previously reported changes.

The model was further characterized by real-time PCR analysis of steady-state mRNA levels of the methionine cycle enzymes, using the 18S gene as reference (Fig. 1A). Severe reductions (70-80%) in MAT1A, BHMT and GNMT transcripts were detected upon galactosamine treatment, whereas mRNA levels for the rest of the enzymes increased; the largest changes corresponded to MAT2A (500%) and MAT2B (250%) transcripts, while more moderate elevations (~150-200%) were detected for MTR and SAHH. Therefore, a *MAT1A* to *MAT2A* expression switch was clearly visible after 48 hours of treatment, the relative expression levels of both transcripts becoming similar (Fig. 1B). Additionally, galactosamine induced the expression of both γ-

glutamylcysteine synthetase (GCL) subunits, modifier (GCLm) and ligase (GCLl), by 350% (Fig. 1A).

The consequences of these expression changes on protein levels were then analyzed in liver cytosols using α-tubulin as reference (Fig. 2A). Reductions (40-45%) in MATα1 and BHMT levels were detected upon galactosamine treatment, whereas SAHH levels increased (190%) and those of GNMT remained unaffected (Fig. 2B). Protein changes were more moderate than in transcript levels, thus putative alterations in mRNA and protein half-lives were explored. For this purpose, we first assessed whether the hepatic effects induced by galactosamine could be reproduced in H35 cells. Cytosolic BHMT protein levels decreased ~30%, whereas those of SAHH increased ~100% in galactosamine-treated cells, following the same trend observed in liver cytosols (Fig. 2C-D). Neither MATα1 nor GNMT were detected in control H35 cells as previously reported, although a faint GNMT band could be observed in cytosols of treated cells (Fig. 2E). Transient transfection with pHA-MAT allowed analysis of HA-MATα1, a tagged-MATα1 that exhibited MAT activity and the expected size and preserved the oligomerization features of MATα1 (Supplementary Fig. S3-5). These transfected cells exhibited a 65% decrease in cytosolic HA-MATα1 levels after galactosamine treatment (Fig. 2F). Altogether, H35 cells reproduced liver behavior, allowing their use to evaluate putative changes in half-life. MAT2B, GCLm and GCLl transcripts increased their half-lives by galactosamine treatment, whereas those of SAHH and BHMT decreased or showed a trend towards reduction, respectively (Supplementary Table S3). In contrast, cytosolic BHMT and SAHH protein half-lives increased 200% by galactosamine treatment (Supplementary Table S3).

Next, changes in representative enzyme activities were measured in liver cytosols (Supplementary Table S1). Total MAT activity (MAT I + MAT II + MAT III)

decreased 50% in the galactosamine group, but no changes were detected using 60 μM methionine and only a tendency towards increase was observed by DMSO activation of MAT III. These activity changes seemed compensated by the reduction in MATα1 protein levels (Fig. 2A). The treated group also showed a 25% reduction in BHMT activity, a modest change compared to alterations in mRNA and protein levels. Evaluation of hepatic metabolite changes by UPLC-MS showed the already mentioned reduction in AdoMet levels in the galactosamine group, together with enhanced levels of Hcy, methionine and, particularly, in GSSG (Supplementary Table S2). These changes caused a 30% decrease in the hepatic methylation index (AdoMet/AdoHcy) and the GSH/GSSG ratio.

Putative changes in the cytosolic association state of hepatic methionine cycle enzymes were evaluated by AGFC, confirming the previously described increase in MAT III activity in the galactosamine group (7), and hence a rise in the calculated dimer/tetramer activity ratio (Supplementary Fig. S2A, C and Supplementary Table S1). Additionally, dot-blot evaluation of MATα1 protein in the column fractions showed a strong reduction in the signal of the galactosamine group, where only MAT III oligomers were detected (Supplementary Fig. S2B, D). Calculated MAT III/I protein ratios were 11.64 ± 3.96 and 24.66 ± 5.38 ($p=0.001$) for control and treated groups, respectively. In contrast, cytosolic SAHH, GNMT and BHMT exhibited no alteration in their association state (Supplementary Fig. S6).

Putative changes on MATα1 subcellular localization induced by galactosamine were then analyzed using initially transiently transfected H35 cells (Fig. 3). Only 15% of the control cells showed nuclear accumulation (N/C>1.2) by indirect immunofluorescence, a percentage that increased to ~60% after galactosamine treatment. In vivo confocal microscopy also demonstrated nuclear accumulation in

~30% and ~90% of the control and galactosamine-treated cells, respectively, whereas controls expressing EGFP showed no alteration in subcellular distribution. MATα1 nuclear accumulation was confirmed by subcellular fractionation showing a 60% increase in HA-MATα1, together with a ~170% increase in nuclear SAHH in the treated group (Fig. 4A, B). Subcellular fractions of control and galactosamine-treated rat livers confirmed the increased nuclear MATα1 (200%) and SAHH (240%) levels, together with an elevated GNMT content (Fig. 4C, D). Immunohistochemistry further reinforced these results showing MATα1 cytoplasmic localization in control livers and nuclear staining in galactosamine-treated tissues (Fig. 5).

Methionine cycle enzymes are oligomers in the cytoplasm, but the nuclear association state has been only determined for MATα1 (50). Therefore, we used AGFC to analyze possible changes in this parameter, and detected that the increased content of GNMT and SAHH in nuclear fractions of galactosamine-treated livers did not involve alterations in their elution pattern (Fig. 6A, B). Calculated elution volumes, 11.76 ml for GNMT and 11.13 ml for SAHH, corresponded to compact homo-tetramers of 133 and 171 kDa, respectively. In contrast, accumulation of nuclear MATα1 in treated livers occurred as tetramers with a parallel reduction in the monomer content (Fig. 6C), and the corresponding decrease in the calculated monomer/tetramer ratios (7.32 ± 2.44 vs. 3.07 ± 1.11; p=0.024) (Fig. 6D). MAT catalysis requires oligomerization, hence the rise in nuclear MAT I content suggested an increase in activity that was in fact detected. Galactosamine treatment resulted in a 250% increase of nuclear MAT activity as compared to the controls (45.67 ± 15.19 vs. 15.82 ± 8.86 pmol/min/mg, p=0.003).

Next, several redox-modulating agents and transiently transfected H35 cells were used to get insight into the mechanisms governing MATα1 subcellular distribution. Reductions in HA-MATα1 cytoplasmic content were found, concomitantly

with nuclear accumulation, upon treatments with galactosamine (~60%; Fig, 7A, C) and BSO (~30%; Fig. 7B, D), an inhibitor of glutathione synthesis. N-acetylcysteine (NAC) and AdoMet prevented galactosamine effects on cytosolic protein levels, whereas nuclear changes were only prevented by NAC (Fig. 7A, C). BSO-induced alterations in HA-MATα1 levels were prevented by EGSH in both subcellular fractions, but not by AdoMet (Fig. 7B, D). Analysis of the glutathione levels and the GSH/GSSG ratio showed that only agents that prevented large alterations in these parameters (NAC and EGSH) were able to maintain the control nucleocytoplasmic distribution (Supplementary Fig. S7). No signs of apoptosis were detected in extracts of the different treatments, according to the lack of caspase-3 activation, but moderate changes in LDH activity in the culture media of galactosamine-treated cells were observed (Supplementary Fig. S8, S9A). The effects described were confirmed in vivo by confocal microscopy using pMAT-EGFP transfected H35 cells and the same agents (Supplementary Fig. S10A). Quantification of the N/C signal ratio indicated 250% increases upon galactosamine or BSO treatments, whereas NAC and EGSH partially prevented the effects on subcellular localization (Supplementary Fig. S10A-C).

An enhanced nuclear capacity to produce AdoMet may be required to support key epigenetic modifications involving methylation, some of which were measured. No significant changes were observed in DNA methylation levels of both rat livers and pHA-MAT-transfected H35 cells, although a trend towards reduction was detected in the galactosamine-treated samples (Fig. 8A, B). In contrast, a 300% increase in me3K27H3 levels was detected in pHA-MAT-transfected cells receiving galactosamine, and NAC prevented this increase (Fig. 8C, D). Therefore, nuclear accumulation of HA-MATα1 correlated positively with me3K27H3 upon galactosamine treatment.

Finally, the effects of acetaminophen (APAP) intoxication on MATα1 nucleocytoplasmic distribution were also examined, given its known effects on methionine metabolism and GSH levels. An acute dose of the drug induced dramatic increases in rat serum transaminase levels (Supplementary Table S4), together with focal necrosis that was visible upon eosin/hematoxylin staining of liver sections (Supplementary Fig. S11). APAP induced significant decreases in hepatic levels of methionine, AdoMet, GSSG and more severe on AdoHcy and GSH that resulted in an increased methylation index, together with a 25% decrease in the GSH/GSSG ratio (Supplementary Table S4). APAP-treated livers showed a 200% elevation of the nuclear MATα1 content, without significant changes in cytoplasmic levels as judged by western blot (Supplementary Fig. S12). In contrast, a 20% decrease in cytosolic MAT activity was detected in the presence of 60 μM or 5 mM methionine, and no significant changes were measured by DMSO activation (Supplementary Table S4). These data suggested an effect of APAP directed towards MAT I activity that was further analyzed by AGFC. Opposite behaviors for dimer/tetramer activity and protein ratios were detected in the cytosol. Thus, while the MAT III/I activity ratio increased 200%, reflecting a decrease in MAT I activity, the protein ratio was reduced by the increased tetramer content (Supplementary Fig. S12C, D). In parallel, the nuclear monomer/tetramer ratio decreased due to a significant increase in MAT I levels, without modification of the total nuclear MAT activity (Supplementary Fig. S12E-G). This lack of changes in nuclear MAT activity presented with a trend towards reduction in hepatic global DNA methylation (Supplementary Fig. S13A). Nuclear accumulation of MATα1-EGFP was also shown by in vivo confocal microscopy in H35-transfected cells upon APAP treatment, an effect that was partially prevented by NAC (Supplementary Fig. S10D, E). APAP, NAC or their combination induced no significant changes in DNA methylation

as compared to cells receiving the vehicle (Supplementary Fig. S13B). However, APAP increased me3K27H3 methylation (200%), an effect that was not prevented by NAC, despite the normalization of glutathione levels and the GSH/GSSG ratio (Supplementary Fig. S7C). Extracts from APAP-treated cells showed activated caspase-3 (19-17 kDa) and increased LDH activity (~170%) in the culture media, suggestive of apoptosis (Supplementary Fig. S8B, S14).

DISCUSSION

Many liver diseases associated with impairment of methionine metabolism proceed with changes in the MAT isoenzymes expressed (*MAT1A* to *MAT2A* switch)(7, 12, 14, 31, 33, 56, 61). By this expression switch the cell changes from high to low V_{max} MAT isoenzymes with the corresponding reductions in MAT activity, AdoMet levels and the methylation index. Additionally, liver injury concurs with decreases in GSH content and/or increases in GSSG, NO concentrations and ROS levels that are known to inhibit cytosolic MAT I/III and, in some cases, change the dimer/tetramer ratio (28, 34, 38, 40, 42, 44, 52, 56). Galactosamine and APAP differ notably in their mechanisms of action (5, 27), but acute doses of both agents induce liver injury with the mentioned alterations in hepatic metabolism (7, 42, 56, 58). Our results confirm these previous observations upon galactosamine treatment, together with a modest increase in *MAT2B* and *MTR* mRNA levels and a strong decrease in *GNMT* and *BHMT* transcripts (Supplementary Fig. S15). These expression changes resemble alterations reported in APAP intoxication, except for *SAHH* and *GNMT* levels that were transiently elevated in this model (56). Protein levels follow the same trend than mRNA in galactosamine intoxication, although more modest alterations are detected, due in some cases to opposite changes in their half-lives. Galactosamine also induces expression of both GCL subunits, whereas APAP and other hepatotoxicants only increase GCLl expression (22, 56). Putative mechanisms by which expression changes take place may involve the presence of antioxidant response elements (AREs) in the corresponding promoters (25), the uridine depletion induced by galactosamine (27), and stabilization/destabilization of the corresponding transcripts through binding to HuR or AUF1, respectively, as has been demonstrated for MAT2A and MAT1A mRNAs during liver carcinogenesis (36, 59).

All these alterations result in reductions of hepatic AdoMet levels in galactosamine and APAP intoxications, as previously described (7, 42, 43, 56, 58). However, AdoHcy and methionine concentrations follow opposite trends in both models, probably due to the combination of divergent changes in SAHH, GNMT, BHMT and MTR expression and protein levels, as well as in the flux through the trans-sulfuration pathway (56). Galactosamine effects in methionine and AdoMet are also supported by the previously reported decreases in ATP and sarcosine levels found in isolated hepatocytes (43). Additionally, decreased AdoMet levels could contribute to this picture by avoiding activation of trans-sulfuration (37, 46), increasing *BHMT* expression (46)(not observed with galactosamine), contributing to methionine and folate recycling by enhancing MTHFR activity and increasing *MTR* expression (57), and modulating HuR nucleocytoplasmic distribution, and hence contributing to increase MAT2A mRNA levels (36). Furthermore, an increased MTFHR activity leads to higher 5-methyltetrahydrofolate levels that inhibit GNMT (32), whereas decreased BHMT levels would result in lower betaine consumption, increasing protection against protein conformational changes (10). **Both drugs lead also to a compensatory increase of GCL expression that should render enhanced total glutathione levels. Nevertheless, such an increase is only observed for galactosamine, probably due to the different detoxification mechanisms used by both drugs. Such mechanisms may require a larger amount of glutathione for APAP metabolization than for galactosamine-derived ROS removal. However, the net results are reduced GSH/GSSG ratios that likely reflect the GSH consumption needed for NAPQI generation** and the GSSG production due to galactosamine-ROS elimination, as well as the galactosamine inhibition of glutathione recycling enzymes (5, 29, 40, 48).

These global effects of galactosamine and APAP on metabolite concentrations reflect mainly cytosolic changes, but may not mirror those in other subcellular compartments with different functions and needs. Classically, methionine metabolism was considered a cytoplasmic pathway and metabolites, such as AdoMet, expected to move to compartments where methylation reactions were held. This hypothesis was supported by the cytoplasmic localization of the enzymes and the existence of AdoMet transporters (23, 33, 45). However, recent reports described nuclear localization of SAHH, GNMT, MATα1, MATα2 and MATβ that was related to in situ production of AdoMet and AdoHcy elimination (26, 49, 50, 60, 62). Hence, the paradigm has changed to propose that enzymes are transported to those locations where metabolite synthesis is needed (16). Nevertheless, the mechanisms involved in the control of their subcellular distribution and their relationship to disease remain unknown. Here, we show that APAP and galactosamine intoxications induce nuclear accumulation of MATα1 and increased MAT I levels that correlate with reduction (galactosamine) or no change (APAP) of the cytosolic protein levels, together with opposite consequences on the MAT III/I protein ratio. Alterations at the protein level only match the total MAT activity of both compartments in galactosamine intoxication, whereas higher MAT I levels in APAP treatment correlate with reduction (cytoplasm) or no effect (nucleus) in this parameter. These differential effects on cytosolic and nuclear MAT activities may rely on the induction of reversible (GSSG, NO and ROS) and/or irreversible (NAPQI) modifications of the protein (4, 5, 42, 53), in the association capacity of the nuclear monomer pool into MAT I and additionally on the moderate APAP dose used.

Epigenetic remodeling is required for the induction/repression of genes involved in defense mechanisms, apoptosis or necrosis during progression of liver damage. The nuclear increase in MAT I induced by galactosamine and APAP may respond to higher

AdoMet needs in this compartment, as reflected by the rise in me3K27H3 levels in H35-treated cells, and the subtle DNA hypomethylation in the galactosamine model. These results confirm previous data associating MATα1 overexpression and changes in me3K27H3 and DNA methylations, as well as the positive correlation between me3K27H3 levels and nucleocytoplamic distribution (50). Additionally, the concomitant elevation of nuclear SAHH and GNMT tetramers, their active assemblies (32, 49), observed in galactosamine-treated livers may contribute to eliminate the resulting AdoHcy and to a fine-tuning of AdoMet levels.

Oxidative stress is among the mechanisms inducing nuclear localization of proteins (21, 41), but it is also involved in the control of epigenetic modifications (13). Galactosamine, APAP and BSO are known to produce oxidative stress, resulting in reduced GSH/GSSG ratios, and all induce nuclear accumulation of MATα1. NAC and EGSH, precursors for GSH synthesis (29), normalize this ratio preventing changes in MATα1 localization induced by the treatments. In contrast, AdoMet, as previously shown (28), is unable to normalize the GSH/GSSG ratio, and hence does not prevent MATα1 nuclear accumulation. These results suggest the implication of a glutathione-dependent mechanism in nuclear localization of MATα1 that for APAP may involve additional processes. Accordingly, NAC does not prevent APAP effects on DNA or me3K27H3 methylations in H35 cells, but increases global DNA methylation in galactosamine-treated cells and prevents the rise in me3K27H3. This positive correlation between nuclear MATα1 levels and me3K27H3, a known repression mark (6), is observed with both drugs, suggesting the need to down-regulate certain genes that may have been activated by the global DNA hypomethylation normally associated with increased *MAT2A* expression (8, 15, 24), and for which our rat models show a trend. Altogether the available results suggest the preference of MAT I to supply AdoMet for

me3K27H3 methylation, whereas MAT II subunits were found interacting with several methyltransferases involved in me2K4H3 and me2K9H3 (26). These epigenetic modifications have been studied specially in cancer and have been associated with either repression (me3K27H3 and me2K9H3) or activation (me2K4H3) of gene expression (55, 51), the final outcomes depending on the genes affected. Overall, changes induced by the treatments on hepatic MATα1 make hepatocytes approach the extrahepatic cell pattern, where this protein is poorly expressed and preferentially localized to the nucleus (50).

In summary, our data indicate that AdoMet homeostasis in liver injury is sustained by changes involving from transcription to activity and subcellular localization of methionine metabolism enzymes. The GSH/GSSG ratio controls MATα1 subcellular distribution, its decrease leading to MAT I nuclear accumulation to supply the increased AdoMet needs for epigenetic remodeling. Concomitantly, SAHH nuclear accumulation contributes to preclude methyltransferase inhibition, maintaining the methylation index. Altogether these findings unveil new implications for the regulation of these enzymes in disease.

INNOVATION

The relationship between changes in subcellular localization of methionine metabolism enzymes and disease was analyzed in acute liver injury. The results demonstrate that S-adenosylmethionine homeostasis is compromised due to a variety of processes, including from changes in expression to altered subcellular distribution of key proteins controlling the S-adenosylmethionine/S-adenosylhomocysteine ratio. Remodeling of methylation-based epigenetic modifications is fulfilled by nuclear accumulation of methionine adenosyltransferase I and S-adenosylhomocysteine hydrolase. Glutathione levels regulate subcellular distribution of these enzymes, effects that are prevented by N-acetylcysteine. These alterations in nucleocytoplasmic localization show a potential as markers of disease.

MATERIALS AND METHODS

Animal models. Male Wistar rats (180-200 g) were divided into four groups (25 animals each) that received i.p. injections at 24 hour intervals of: PBS (control 1 and 2 groups), D-galactosamine hydrochloride (400 mg/kg; Sigma, St. Louis MO) or APAP (250 mg/kg; Sigma). Animals were sacrificed after 24 (control 1 and APAP groups) or 48 hours (control 2 and galactosamine groups) and blood, liver and kidneys extracted. Tissues were processed immediately for subcellular fractionation or frozen in liquid nitrogen for storage at –80ºC. All animals were treated according to the Guidelines for Animal Experimentation of the CSIC and the European Union.

Histology and immunohistochemistry. Liver samples and one kidney of each individual were fixed in formaldehyde 10% (v/v) before being embedded in paraffin. Sections (10 microns) were prepared and used for morphological analysis after standard hematoxylin/eosine staining.

Immunohistochemistry was performed on paraffin sections (5 μm) using anti-MATα1 or preimmune rabbit sera (1:1000, v/v), followed by EnVision (DAKO Corporation, Carpinteria CA) as previously described (50). Counterstaining was performed with hematoxylin. Sections were photographed and analyzed using Adobe-Photoshop CS software v. 8.0.1.

Liver function analysis. Serum samples were obtained by standard protocols after incubation at 37ºC for 20-30 minutes. Transaminase levels were analyzed at the Centro de Análisis Sanitarios of the Universidad Complutense de Madrid (Facultad de Farmacia, Madrid, Spain).

Plasmids, expression and characterization of tagged proteins. The pHA(del) plasmid was prepared by deletion of C876 of pCMV-HA (Clontech, Mountain View CA) to allow in-frame cloning of the rat *MAT1A* ORF that was obtained by EcoRI/NotI

(Invitrogen-Life Technologies, Carlsbad CA) digestion of pSSRL-BlueT2 (1). The resulting plasmid was named pHA-MAT. The HA-MATα1 protein contains the LMAMEAEFH linker sequence, increasing its size by ~2 kDa. Protein characterization was carried out by MAT activity determinations (160 μl), western blot (80 μg) and analytical gel filtration chromatography (100 μl) using the soluble fraction obtained after overexpression into BL21(DE3) cells, as previously described (2, 50). The results were compared with soluble fractions of cells transformed with pHA(del) (Supplementary Fig. S3-S5). Additional plasmids used in this work, pFLAG-MAT and pMAT-EGFP, were previously described and both FLAG-MATα1 and MATα1-EGFP proteins characterized (50).

Cell culture and treatments. Rat hepatoma H35 cells were grown in DMEM medium (Gibco-Life Technologies) containing 10% (v/v) FBS and 2 mM glutamine. Transient transfections with pFLAG-MAT, pMAT-EGFP or pHA-MAT constructs were carried out using Lipofectamine for 6-8 hours (Invitrogen-Life Technologies). Concentrations of the agents (Sigma) used in the treatments were as follows: 10 mM D-galactosamine (Gal); 5 mM NAC; 0.5 mM AdoMet chloride; 1 mM BSO; 1 mM EGSH; and 5 mM APAP. All the agents were diluted in PBS, except for APAP that was dissolved in ethanol (1% v/v final concentration). BSO and APAP treatments were carried out for 24 hours, whereas galactosamine was added for 48 hours. NAC was added 12 hours before galactosamine or APAP, whereas AdoMet and EGSH were supplied 15 min prior to either galactosamine or BSO administration.

For half-life experiments H35 cells (300000 cells) were seeded and grown overnight. Three plates per time point were prepared containing either PBS (controls) or D-galactosamine (treated) for 48 hours. The culture medium was then replaced with serum-free medium and 20 μg/ml cycloheximide (Sigma) or 5 μg/ml actinomycin D

(Sigma) added to the plates. Samples were collected at different time points up to 24 hours to obtain either the cytosolic fractions or total RNA, and the effects on each protein or mRNA were analyzed by western blot or real-time RT-PCR, respectively. The values were corrected against α-tubulin (western blot) or the 18S transcript, and the half-lives calculated using GraphPad Prism v. 5.0.

Confocal microscopy. H35 cells were grown on coverslips for indirect immunofluorescence (40000 cells) or in vivo (100000 cells) confocal microscopy and transient transfections with pFLAG-MAT or pMAT-EGFP carried out before treatment, using the conditions described above. Nuclei were stained for 1 hour using Hoechst 33342 (5 μg/ml; Molecular Probes, Carlsbad CA) before cell fixation or direct observation. Fixation was carried out using 2% (v/v) formaldehyde, followed by permeabilization using 0.3% (v/v) Triton X-100 (Calbiochem-Merck, Darmstadt, Germany) as previously described (50). Fixed cells were incubated for 1 hour sequentially with monoclonal mouse M2 anti-FLAG (5 μg/ml; Sigma) and anti-mouse-Alexa Fluor 488 (Molecular Probes). Glass coverslips were mounted using Prolong Gold anti-fade reagent (Invitrogen). Cell imaging (0.3-0.4 μm sections) was performed on a Leica TCS SPII Spectral microscope using a 63x/1.3 NA objective at the Confocal Microscopy facilities of the Universidad Autónoma de Madrid (UAM). Images were analyzed using the Leica Confocal Software (LCS Lite, Zurich, Switzerland).

Subcellular fractionation. Rat liver samples were homogenized in 4 volumes of 10 mM Tris/HCl pH 7.4 containing 0.3 M sucrose, 0.1 mM EGTA, 0.1% 2-mercaptoethanol (Merck, Darmstadt, Germany), 1 mM benzamidine (Sigma), 0.1 mM PMSF (Sigma) and 10 μg/ml soybean trypsin inhibitor (Sigma). Homogenates were centrifuged at 12500 xg for 15 min at 4ºC and the supernatants ultracentrifuged at

105000 xg for 1 hour at 4ºC. This second supernatant, the cytosolic fraction, was used for activity measurements, AGFC and Western blot.

Separation of nuclear and cytoplasmic fractions was carried out in the absence of detergents as previously described (3, 50). For this purpose, liver samples (~8 g) or H35 cells (2 x10^6/p100), wild type and transiently transfected with pFLAG-MAT or pHA-MAT, were used. Samples of subcellular fractions were utilized for western blot, AGFC and activity determinations. Cross-contamination among fractions was monitored by measuring LDH activity as described previously (50), and by densitometric scanning of the immunoblot signals for the marker proteins α-tubulin (cytoplasm) and lamin B1 (nucleus) and found to be <0.08%. Cell extracts for evaluation of histone methylation were obtained by a 30 minute incubation on ice in 50 mM Tris/HCl pH 7.5, 150 mM NaCl, 0.5% (v/v) SDS, 30 mM sodium pyrophosphate, 50 mM NaF and protease inhibitors, followed by centrifugation at 100000 xg 30 minutes.

Quantitative RT-PCR. Total RNA was isolated from livers of control and treated animals using the RNeasy kit (Qiagen, Hilden, Germany), and the quality and quantity determined spectrometrically and by automated electrophoretogram on a Bioanalyzer 2100. Reverse transcription and PCR were done as previously described using 1.25 μg of total RNA as template and the High Capacity Archive kit (Applied Biosystems-Life Technologies)(14). The cDNAs (10 ng) were amplified in triplicate using gene specific primers (Supplementary Table 5) and Power SYBR Green PCR Master Mix (Applied Biosystems) using the ABI 7900HT Real-Time PCR system (Applied Biosystems) at the Genomic Service of the Instituto de Investigaciones Biomédicas "Alberto Sols" (CSIC-UAM). Fluorescent signals were collected after each extension step, and the curves analyzed with SDS 2.2.2 software. Relative expression ratios were normalized to the geometric mean of the 18S gene used as a control.

Experimental efficiencies were calculated for each transcript and used to obtain the fold changes according to Pfaffl (47).

Activity measurements. Samples of the subcellular fractions were used to determine MAT, BHMT and LDH activities as described previously (18, 19, 50). Briefly, cytosolic MAT activity measurements were carried out for 30 min using 160 μl samples and three types of reaction mixtures that differ mainly in their methionine (Sigma) content: i) 5 mM (total activity; standard mixture); ii) 60 μM (MAT I and MAT II activities); and iii) 60 μM plus 10% (v/v) DMSO (MAT I, MAT II and stimulated MAT III activities). MAT activity measurements in AGFC fractions (100 μl) and nuclear extracts (160 μl) were performed using the standard mixture for 30 minutes and 2 hours, respectively. For BHMT activity determinations, cytosols (75 μl) were used and reactions carried out for 30 minutes. LDH activity was followed at 340 nm and 37ºC for 5 min using subcellular fractions (10-100 μl) or culture media (100 μl) in 50 mM Tris/HCl pH 7.5, 0.2 mM NADH (Sigma) and 1 mM sodium pyruvate (Sigma).

Analytical gel filtration chromatography (AGFC). Subcellular fractions (100 μl) were loaded on a Superose 12 10/300 GL column (GE Healthcare, Barcelona, Spain) equilibrated and eluted at 0.3 ml/min in 50 mM Tris/HCl pH 8, 10 mM $MgSO_4$, 1 mM EDTA containing 150 mM KCl. Fractions (210 μl) were collected for activity measurements and/or dot-blot analyses. Standards (GE Healthcare and Sigma) for column calibration and their elution volumes are indicated in the figure legends.

Western blot and Dot blot. Liver cytosols (25 μg) or H35 cytosolic samples (80 μg) and nuclear fractions (150 μg) were loaded on 10% SDS-PAGE gels and transferred to nitrocellulose membranes (GE Healthcare) for incubation with antibodies against: MATα1 (1:10000 v/v)(31), BHMT (1:20000 v/v)(19), SAHH (1:1000 v/v; Santa Cruz sc-55759, Santa Cruz CA), GNMT (1:1000 v/v; Santa Cruz sc-68871),

FLAG (2.5 μg/ml; Sigma), HA (1:1000 v/v; Covance, Madrid, Spain), α-tubulin (1:2500 v/v; Sigma) or lamin B1 (1:1000 v/v; Abcam, Cambridge, UK). In contrast, evaluation of caspase-3 activation (50 μg/lane) and histone methylation (10 μg/lane) were performed on 14% SDS-PAGE gels and western blots incubated with anti-caspase-3 (1:1000 v/v; Cell Signalling, Danvers MA) or anti-me3K27H3 (1 μg/ml; Upstate-Millipore, Charlottesville VA), respectively. Western blot signals were developed using the Western Lightning Chemiluminescence Reagent (Perkin Elmer Life Sciences, Waltham MA) and densitometric scanning was carried out using ImageJ v. 1.37 (http://rsb.info.nih.gov/ij/). Values were normalized against the α-tubulin or lamin B1 controls for comparison.

For Dot blot analysis aliquots (100 μl) of the column fractions were spotted onto nitrocellulose membranes as previously described (54), and incubated with the antibodies of interest using the same dilutions as for western blot.

Analysis of metabolite levels. Quantification of metabolite levels was performed, as previously described, at OWL Genomics facilities (Derio, Vizcaya, Spain)(14). Briefly, tissue samples were homogenized in 0.4 M perchloric acid and the supernatant used to determine reduced (GSH) and oxidized (GSSG) glutathione levels. AdoMet, AdoHcy, Hcy and methionine were measured after 6-aminoquinolyl-N-hydroxysuccinimidyl carbamate derivatization using the AccQ Tag Ultra derivatization kit (Waters, Milford MA). Samples were analyzed at 50ºC using a BEH C18 column (Waters) and a gradient from 0.05% formic acid: water (buffer A) to 0.05% formic acid: acetonitrile (buffer B) coupled to ESI detection (UPLC-MS). Glutathione levels in H35-treated cells were determined by the method of Tietze.

Global DNA methylation. Genomic DNA from liver samples or H35 cells was extracted using the DNeasy kit (Qiagen). The quality and quantity of the purified DNA

was determined spectrophotometrically (A_{260}/A_{280} ratio). Samples (200 ng/well) were used to determine global DNA methylation levels using the IMPRINT® Methylation DNA Quantification kit (Sigma) following manufacturer's instructions.

Protein concentration determinations. Protein concentration was measured using the BioRad protein assay and bovine serum albumin as the standard.

Statistics. GraphPad Prism v. 5.0 (GraphPad Software) was used for statistical analysis of the data. Experiments containing two groups of data were analyzed using Student's t-test for independent samples, whereas one-way ANOVA with Bonferroni post-hoc test was preferred for multiple comparisons; differences were considered significant when $p \leq 0.05$.

ACKNOWLEDGMENTS

This work was supported by grants of the Ministerio de Economía y Competitividad (BFU2005-00050, BFU2008-00666 and BFU2009-08977 to MAP, SAF2009-11642 and SAF2012-36519 to DP-S and PS09/01762 to JP-M) and the Instituto de Salud Carlos III (RCMN C03/08 and PI05/0563 to MAP, RD07/0064/0007 and RD12/0013/0008 to DP-S). M. D. was supported by fellowships of RCMN C03/08 and PI05/0563 and M. P. by BFU2009-08977. The authors thank A. Cerro, D. Arroyo and Y. López-Gordillo for their help with histological techniques.

No competing financial interests exist.

LIST OF ABBREVIATIONS

AdoHcy, S-adenosylhomocysteine

AdoMet, S-adenosylmethionine

AGFC, analytical gel filtration chromatography

APAP, acetaminophen

BHMT, betaine homocysteine methyltransferase

BSO, buthionine sulfoximine

EGFP, enhanced green fluorescence protein

EGSH, glutathione ethyl ester

Gal, D-galactosamine

GCL, γ-glutamylcysteine synthetase

GNMT, glycine N-methyltransferase

GSH, glutathione reduced form

GSSG, glutathione oxidized form

HCC, hepatocellular carcinoma

Hcy, homocysteine

HuR, human antigen R

MafK, Maf oncoprotein K

MAT, methionine adenosyltransferase

me2K4H3, histone 3 K4 dimethylation

me2K9H3, histone 3 K9 dimethylation

me3K27H3, histone 3 K27 trimethylation

MTHFR, methylene tetrahydrofolate reductase

MTR, methionine synthase

NAC, N-acetylcysteine

NAPQI, N-acetyl-*p*-benzoquinone imine

N/C, nuclear to cytoplasmic signal ratio

NO, nitric oxide

UPLC-MS, ultraperformance liquid chromatography- mass spectrometry

ROS, reactive oxygen species

SAHH, S-adenosylhomocysteine hydrolase

REFERENCES

1. Alvarez L, Asuncion M, Corrales F, Pajares MA, and Mato JM. Analysis of the 5' non-coding region of rat liver S-adenosylmethionine synthetase mRNA and comparison of the Mr deduced from the cDNA sequence and the purified enzyme. *FEBS Lett* 290: 142-146, 1991.

2. Alvarez L, Mingorance J, Pajares MA, and Mato JM. Expression of rat liver S-adenosylmethionine synthetase in Escherichia coli results in two active oligomeric forms. *Biochem J* 301: 557-561, 1994.

3. Andrews NC, and Faller DV. A rapid micropreparation technique for extraction of DNA-binding proteins from limiting numbers of mammalian cells. *Nucleic Acids Res* 19: 2499, 1991.

4. Avila MA, Mingorance J, Martinez-Chantar ML, Casado M, Martin-Sanz P, Bosca L, and Mato JM. Regulation of rat liver S-adenosylmethionine synthetase during septic shock: role of nitric oxide. *Hepatology* 25: 391-396, 1997.

5. Baillie TA, and Rettie AE. Role of biotransformation in drug-induced toxicity: influence of intra- and inter-species differences in drug metabolism. *Drug Metab Pharmacokinet* 26: 15-29, 2011.

6. Bhaumik SR, Smith E, and Shilatifard A. Covalent modifications of histones during development and disease pathogenesis. *Nat Struct Mol Biol* 14: 1008-1016, 2007.

7. Cabrero C, Duce AM, Ortiz P, Alemany S, and Mato JM. Specific loss of the high-molecular-weight form of S-adenosyl-L-methionine synthetase in human liver cirrhosis. *Hepatology* 8: 1530-1534, 1988.

8. Cai J, Mao Z, Hwang JJ, and Lu SC. Differential expression of methionine adenosyltransferase genes influences the rate of growth of human hepatocellular carcinoma cells *Cancer Res* 58: 1444-1450, 1998.

9. Cantoni GL. Biological methylation: selected aspects. *Annu Rev Biochem* 44: 435-451, 1975.

10. Chow MK, Devlin GL, and Bottomley SP. Osmolytes as modulators of conformational changes in serpins. *Biol Chem* 382: 1593-1599, 2001.

11. Corrales F, Gimenez A, Alvarez L, Caballeria J, Pajares MA, Andreu H, Pares A, Mato JM, and Rodes J. S-adenosylmethionine treatment prevents carbon tetrachloride-induced S-adenosylmethionine synthetase inactivation and attenuates liver injury. *Hepatology* 16: 1022-1027, 1992.

12. Corrales F, Ochoa P, Rivas C, Martin-Lomas M, Mato JM, and Pajares MA. Inhibition of glutathione synthesis in the liver leads to S-adenosyl-L-methionine synthetase reduction. *Hepatology* 14: 528-533, 1991.

13. Cyr AR, and Domann FE. The redox basis of epigenetic modifications: from mechanisms to functional consequences. *Antioxid Redox Signal* 15: 551-589, 2011.

14. Delgado M, Perez-Miguelsanz J, Garrido F, Rodriguez-Tarduchy G, Perez-Sala D, and Pajares MA. Early effects of copper accumulation on methionine metabolism. *Cell Mol Life Sci* 65: 2080-2090, 2008.

15. Ehrlich M. DNA hypomethylation in cancer cells. *Epigenomics* 1: 239-259, 2009.

16. Gibson BA, and Kraus WL. Small molecules, big effects: a role for chromatin-localized metabolite biosynthesis in gene regulation. *Mol Cell* 41: 497-499, 2011.

17. Gil B, Casado M, Pajares MA, Bosca L, Mato JM, Martin-Sanz P, and Alvarez L. Differential expression pattern of S-adenosylmethionine synthetase isoenzymes during rat liver development. *Hepatology* 24: 876-881, 1996.

18. Gil B, Pajares MA, Mato JM, and Alvarez L. Glucocorticoid regulation of hepatic S-adenosylmethionine synthetase gene expression. *Endocrinology* 138: 1251-1258, 1997.

19. Gonzalez B, Campillo N, Garrido F, Gasset M, Sanz-Aparicio J, and Pajares MA. Active-site-mutagenesis study of rat liver betaine-homocysteine S-methyltransferase. *Biochem J* 370: 945-952, 2003.

20. Gonzalez B, Garrido F, Ortega R, Martinez-Julvez M, Revilla-Guarinos A, Perez-Pertejo Y, Velazquez-Campoy A, Sanz-Aparicio J, and Pajares MA. NADP(+) Binding to the Regulatory Subunit of Methionine Adenosyltransferase II Increases Intersubunit Binding Affinity in the Hetero-Trimer. *PloS ONE* 7: e50329, 2012.

21. Hara MR, and Agrawal N, Kim SF, Cascio MB, Fujimuro M, Ozeki Y, Takahashi M, Cheah JH, Tankou SK, Hester LD, Ferris CD, Hayward SD, Snyder SH, and Sawa A. S-nitrosylated GAPDH initiates apoptotic cell death by nuclear translocation following Siah1 binding. *Nat Cell Biol* 7: 665-674, 2005.

22. Heijne WH, Jonker D, Stierum RH, van Ommen B, and Groten JP. Toxicogenomic analysis of gene expression changes in rat liver after a 28-day oral benzene exposure. *Mut Res* 575: 85-101, 2005.

23. Horne DW, Holloway RS, and Wagner C. Transport of S-adenosylmethionine in isolated rat liver mitochondria. *Arch Biochem Biophys* 343: 201-206, 1997.

24. Huang ZZ, Mato JM, Kanel G, and Lu SC. Differential effect of thioacetamide on hepatic methionine adenosyltransferase expression in the rat *Hepatology* 29: 1471-1478, 1999.

25. Jaiswal AK. Nrf2 signaling in coordinated activation of antioxidant gene expression. *Free Radic Biol Med* 36: 1199-1207, 2004.

26. Katoh Y, Ikura T, Hoshikawa Y, Tashiro S, Ito T, Ohta M, Kera Y, Noda T, and Igarashi K. Methionine Adenosyltransferase II Serves as a Transcriptional Corepressor of Maf Oncoprotein. *Mol Cell* 41: 554-566, 2011.

27. Keppler DO, Pausch J, and Decker K. Selective uridine triphosphate deficiency induced by D-galactosamine in liver and reversed by pyrimidine nucleotide precursors. Effect on ribonucleic acid synthesis. *J Biol Chem* 249: 211-216, 1974.

28. Kucera O, Cervinkova Z, Lotkova H, Krivakova P, Rousar T, Muzakova V, Hezova R, Kandar R, and Rudolf E. Protective effect of S-adenosylmethionine against galactosamine-induced injury of rat hepatocytes in primary culture. *Physiol Res* 55: 551-560, 2006.

29. Lu SC. Regulation of glutathione synthesis. *Mol Aspects Med* 30: 42-59, 2009.

30. Lu SC, Alvarez L, Huang ZZ, Chen L, An W, Corrales FJ, Avila MA, Kanel G, and Mato JM. Methionine adenosyltransferase 1A knockout mice are predisposed to liver injury and exhibit increased expression of genes involved in proliferation. *Proc Natl Acad Sci USA* 98: 5560-5565, 2001.

31. Lu SC, and Mato JM. S-adenosylmethionine in liver health, injury, and cancer. *Physiol Rev* 92: 1515-1542, 2012.

32. Luka Z, Mudd SH, and Wagner C. Glycine N-methyltransferase and regulation of S-adenosylmethionine levels. *J Biol Chem* 284: 22507-22511, 2009.

33. Markham GD, and Pajares MA. Structure-function relationships in methionine adenosyltransferases. *Cell Mol Life Sci* 66: 636-648, 2009.

34. Martinez-Chantar ML, and Pajares MA. Role of thioltransferases on the modulation of rat liver S-adenosylmethionine synthetase activity by glutathione. *FEBS Lett* 397: 293-297, 1996.

35. Martinez-Chantar ML, Vazquez-Chantada M, Ariz U, Martinez N, Varela M, Luka Z, Capdevil A, Rodriguez J, Aransay AM, Matthiesen R, Yang H, Calvisi DF, Esteller M, Fraga M, Lu SC, Wagner C, and Mato JM. Loss of the glycine N-methyltransferase gene leads to steatosis and hepatocellular carcinoma in mice. *Hepatology* 47: 1191-1199, 2008.

36. Martinez-Chantar ML, Vazquez-Chantada M, Garnacho M, Latasa MU, Varela-Rey M, Dotor J, Santamaria M, Martinez-Cruz LA, Parada LA, Lu SC, and Mato JM. S-adenosylmethionine regulates cytoplasmic HuR via AMP-activated kinase. *Gastroenterology* 131: 223-232, 2006.

37. Mato JM, Alvarez L, Ortiz P, and Pajares MA. S-adenosylmethionine synthesis: molecular mechanisms and clinical implications. *Pharmacol Ther* 73: 265-280, 1997.

38. McMillan JM, and Jollow DJ. Galactosamine hepatotoxicity: effect of galactosamine on glutathione resynthesis in rat primary hepatocyte cultures. *Toxicol Appl Pharmacol* 115: 234-240, 1992.

39. Mudd SH, Brosnan JT, Brosnan ME, Jacobs RL, Stabler SP, Allen RH, Vance DE, and Wagner C. Methyl balance and transmethylation fluxes in humans. *Amn J Clin Nutr* 85:19-25, 2007.

40. Okada T, Kawakami S, Nakamura Y, Han KH, Ohba K, Aritsuka T, Uchino H, Shimada K, Sekikawa M, Ishii H, and Fukushima M. Amelioration of D-

galactosamine-induced acute liver injury in rats by dietary supplementation with betaine derived from sugar beet molasses. *Biosci Biotechnol Biochem* 75: 1335-1341, 2011.

41. Okamoto K, Tanaka H, Ogawa H, Makino Y, Eguchi H, Hayashi S, Yoshikawa N, Poellinger L, Umesono K, and Makino I. Redox-dependent regulation of nuclear import of the glucocorticoid receptor. *J Biol Chem* 274: 10363-10371, 1999.

42. Ozturk M, Lemonnier F, Cresteil D, and Lemonnier A. Changes in methionine metabolism induced by D-galactosamine in isolated rat hepatocytes. *Biochem Pharmacol* 35: 4223-4228, 1986.

43. Ozturk M, Lemonnier F, Cresteil D, Scotto J, and Lemonnier A. Methionine metabolism and ultrastructural changes with D-galactosamine in isolated rat hepatocytes. *Chem Biol Interact* 51: 63-76, 1984.

44. Pajares MA, Duran C, Corrales F, Pliego MM, and Mato JM. Modulation of rat liver S-adenosylmethionine synthetase activity by glutathione. *J Biol Chem* 267: 17598-17605, 1992.

45. Pajares MA, and Markham GD. Methionine adenosyltransferase (S-adenosylmethionine synthetase). *Adv Enzymol Relat Areas Mol Biol* 78: 449-521, 2011.

46. Pajares MA, and Perez-Sala D. Betaine homocysteine S-methyltransferase: just a regulator of homocysteine metabolism? *Cell Mol Life Sci* 63: 2792-2803, 2006.

47. Pfaffl MW. A new mathematical model for relative quantification in real-time RT-PCR. *Nucleic Acids Res* 29,: e45, 2001.

48. Quintero A, Pedraza CA, Siendones E, Kamal ElSaid AM, Colell A, Garcia-Ruiz C, Montero JL, De la Mata M, Fernandez-Checa JC, Mino G, and Muntane J. PGE1 protection against apoptosis induced by D-galactosamine is not related to the modulation of intracellular free radical production in primary culture of rat hepatocytes. *Free Radic Res* 36: 345-355, 2002.

49. Radomski N, Kaufmann C, and Dreyer C. Nuclear accumulation of S-adenosylhomocysteine hydrolase in transcriptionally active cells during development of Xenopus laevis. *Mol Biol Cell* 10: 4283-4298, 1999.

50. Reytor E, Perez-Miguelsanz J, Alvarez L, Perez-Sala D, and Pajares MA. Conformational signals in the C-terminal domain of methionine adenosyltransferase I/III determine its nucleocytoplasmic distribution. *FASEB J* 23: 3347-3360, 2009.

51. Rodriguez-Paredes M, and Esteller M. Cancer epigenetics reaches mainstream oncology. *Nat Med* 17: 330-339, 2011.

52. Ruiz F, Corrales FJ, Miqueo C, and Mato JM. Nitric oxide inactivates rat hepatic methionine adenosyltransferase In vivo by S-nitrosylation. *Hepatology* 28: 1051-1057, 1998.

53. Sanchez-Gongora E, Ruiz F, Mingorance J, An W, Corrales FJ, and Mato JM. Interaction of liver methionine adenosyltransferase with hydroxyl radical. *FASEB J* 11: 1013-1019, 1997.

54. Sanchez-Perez GF, Gasset M, Calvete JJ, and Pajares MA. Role of an intrasubunit disulfide in the association state of the cytosolic homo-oligomer methionine adenosyltransferase. *J Biol Chem* 278: 7285-7293, 2003.

55. Sandoval J, and Esteller M. Cancer epigenomics: beyond genomics. *Curr Opin Genet Dev* 22: 50-55, 2012.

56. Schnackenberg LK, Chen M, Sun J, Holland RD, Dragan Y, Tong W, Welsh W, and Beger RD. Evaluations of the trans-sulfuration pathway in multiple liver toxicity studies. *Toxicol Appl Pharmacol* 235: 25-32, 2009.

57. Stover PJ. One-carbon metabolism-genome interactions in folate-associated pathologies. *J Nutr* 139: 2402-2405, 2009.

58. Stramentinoli G, Gualano M, and Ideo G. Protective role of S-adenosyl-L-methionine on liver injury induced by D-galactosamine in rats. *Biochem Pharmacol* 27: 1431-1433, 1978.

59. Vazquez-Chantada M, Fernandez-Ramos D, Embade N, Martinez-Lopez N, Varela-Rey M, Woodhoo A, Luka Z, Wagner C, Anglim PP, Finnell RH, Caballeria J, Laird-Offringa IA, Gorospe M, Lu SC, Mato JM, and Martinez-Chantar ML. HuR/Methyl-HuR and AU-Rich RNA Binding Factor 1 Regulate the Methionine Adenosyltransferase Expressed During Liver Proliferation, Differentiation, and Carcinogenesis. *Gastroenterology* 138: 1943-1953, 2010.

60. Xia M, Chen Y, Wang LC, Zandi E, Yang H, Bemanian S, Martinez-Chantar ML, Mato JM, and Lu SC. Novel function and intracellular localization of methionine adenosyltransferase 2{beta} splicing variants. *J Biol Chem* 285: 20015-20021, 2010.

61. Yang H, Sadda MR, Yu V, Zeng,Y, Lee TD, Ou X, Chen L, and Lu SC. Induction of human methionine adenosyltransferase 2A expression by tumor necrosis factor alpha. Role of NF-kappa B and AP-1. *J Biol Chem* 278: 50887-50896, 2003.

62. Yeo EJ, and Wagner C. Tissue distribution of glycine N-methyltransferase, a major folate-binding protein of liver. *Proc Natl Acad Sci USA* 91: 210-214, 1994.

FIGURE LEGENDS

FIG. 1. Analysis of expression changes by real-time RT-PCR. Changes in steady-state mRNA levels of enzymes of the hepatic methionine cycle and glutathione synthesis induced by D-galactosamine were analyzed by real-time RT-PCR. (A) Fold change in the galactosamine-treated group (N=16) calculated against the control group (N=16) using the 18S gene as reference (mean ± SD). Statistical evaluation was performed using ratios for each transcript vs. 18S (*$p<0.05$). (B) MAT transcript changes (mean ± SD) within control (left) and galactosamine (right) groups using control MTR levels as reference for graphical purposes. Multiple comparisons were performed and changes considered significant when $p<0.05$ (*vs. control MAT1A; ** vs. control MAT2A; *** vs. control MAT2B).

FIG. 2. **Western blot analysis of cytosolic methionine cycle enzymes.** Samples of liver cytosols (25 μg) from control (N=16) and galactosamine-treated (N=16) rats were used for immunoblotting. (A) Representative blots of animals in each group. (B) Quantification of the signals for each protein corrected against α-tubulin (mean ± SD) of animals in the control (black bars) and galactosamine groups (white bars). (C-E) Results from wild type and (F) pHA-MAT transiently transfected H35 cells treated with PBS (control) or galactosamine (gal). Cytoplasmic samples (20-30 μg/lane) were used for immunoblotting using anti-BHMT (C), anti-SAHH (D), anti-GNMT (E) or anti-HA (F) and anti-α-tubulin (loading control). Student's t-tests of the data were performed against the corresponding control group (*$p \leq 0.05$).

FIG. 3. In vivo and indirect fluorescence confocal microscopy of transiently transfected H35 cells after D-galactosamine treatment. Hepatoma H35 cells were transiently transfected with pFLAG, pFLAG-MAT, pEGFP or pMAT-EGFP. The plates were divided into two groups that were treated for 48 hours with PBS (control) or 10

mM galactosamine. Representative examples of the expression of tagged-MATα1 in control and treated cells visualized by confocal microscopy are shown. (A) Indirect immunofluorescence of FLAG-MATα1 localization using anti-FLAG. (B) In vivo results with MATα1-EGFP. Colocalization with nuclear staining is shown in white (bar scale, 25 μm). Histograms show quantification of the nucleo/cytoplasmic ratio (mean ± SD) obtained with FLAG (C) and EGFP (D) transfected cells of five independent experiments carried out in triplicate (*p≤ 0.05). C=N when N/C=1 ± 0.2. To see this illustration in color the reader is referred to the web version of this article at www.liebertonline.com/ars

FIG. 4. Western blot analysis of nuclear fractions. Nuclear fractions (100 μg/lane) of pHA-MAT and wild type transfected H35 cells were analyzed by western blot using anti-HA (A) or anti-SAHH (B), anti-tubulin and anti-lamin B1 as cytoplasmic and nuclear markers, respectively. Signals were quantified and corrected against lamin B1 for comparison (mean ± SD). Representative blots of five independent experiments carried out in triplicate are shown. (C) Representative immunoblots of liver nuclear fractions from control (N=6) and galactosamine (N=6) treated rats incubated with the antibodies indicated on the left. (D) Quantification of the blots (mean ± SD). Statistical analysis was performed by Student's t-test (* p≤ 0.05).

FIG. 5. Subcellular distribution of MATα1 in liver samples analyzed by immunohistochemistry. Paraffin sections (5 μm thick) of liver samples from control and D-galactosamine-treated rats were incubated with anti-MATα1 or preimmune sera and counterstained with hematoxylin. Preimmune serum gave no signal in control (A), and galactosamine-treated livers (B,C). In contrast, anti-MATα1 signal was detected in hepatocyte cytosols of control (D) and galactosamine livers (E,F), whereas a mixture of positive (arrows) and negative (arrowheads) nuclear staining was visible in the treated

samples. Panels C and F show a lower magnification view of the liver sections. Scale bars correspond to 10 μm (A,B,D,E) and 25 μm (C,F). To see this illustration in color the reader is referred to the web version of this article at www.liebertonline.com/ars

FIG. 6. Analysis of the association state of nuclear methionine metabolism enzymes. Livers of control (C; N=10) and galactosamine-treated rats (Gal; N=8) were used for subcellular fractionation. Representative AGFC profiles of nuclear fractions of control and treated animals obtained by dot-blot analysis are shown: (A) anti-GNMT, (B) anti-SAHH, (C) anti-MATα1. Elution positions for tetramers (T) and monomers (M) are indicated. (D) MAT monomer/tetramer ratio (mean ± SD) calculated from the dot-blot data of six independent experiments carried out in duplicate. Data were analyzed by Students t-tests (*p≤ 0.05). Protein standards used for column calibration and their elution volumes were as follows: blue dextran (2000 kDa; 7.13 ml), apoferritin (443 kDa; 9.55 ml), β-amylase (200 kDa; 10.38 ml), alcohol dehydrogenase (150 kDa; 11.05 ml), conalbumin (75 kDa; 11.88 ml), ovalbumin (43 kDa; 12.5 ml), carbonic anhydrase (29 kDa; 13 ml) and ATP (551 Da; 17.39 ml).

FIG. 7. Effect of redox-modulating agents on H35 cells. Cytosolic and nuclear fractions of hepatoma H35 cells transiently transfected with pHA-MAT, and incubated with the agents indicated in the figure, were analyzed by western blot. Representative western blots of eleven independent experiments are shown together with quantification of the data; (A,B) cytosolic HA-MATα1/tubulin and (C,D) nuclear HA-MATα1/lamin B1 ratios. Histograms present the results (mean ± SD) as percentage of the control (PBS). Multiple comparisons were performed with ANOVA vs. control (*p≤0.05) and BSO or D-galactosamine (Gal; **p≤0.05).

FIG. 8. Effects of redox-modulating agents on nuclear methylations. (A) Global DNA methylation levels (mean ± SD) from control (N=6) and galactosamine-

treated livers (N=6). (B, C) Hepatoma H35 cells transiently transfected with pHA or pHA-MAT and treated with the indicated agents were used to obtain genomic DNA or cell extracts. (B) Global DNA methylation levels (mean ± SD) from treated cells were calculated from data of three independent experiment carried out in triplicate using a standard curve of methylated control DNA. Multiple comparisons were performed with ANOVA (*p≤0.05 vs. pHA; ** vs. PBS; *** vs. Gal). (C) Representative immunoblots of me3K27H3 levels from four independent experiments carried out in triplicate are shown. The mobility and size of the standards is indicated on the right. (D) Quantification of me3K27H3 signals corrected against HA-MATα1 levels (mean ± SD); tubulin signals were used as loading controls. Multiple comparison were performed with ANOVA and differences were considered significant when p≤0.05 (* vs. PBS; ** vs. Gal).

A

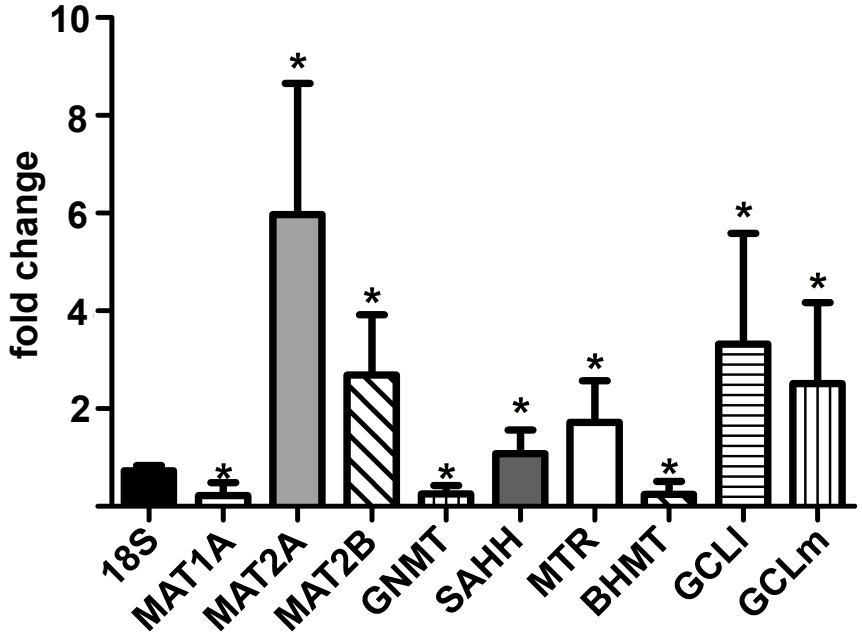
fold change
10
8
6
4
2
18S
MAT1A
MAT2A
MAT2B
GNMT
SAHH
MTR
BHMT
GCLI
GCLm

B

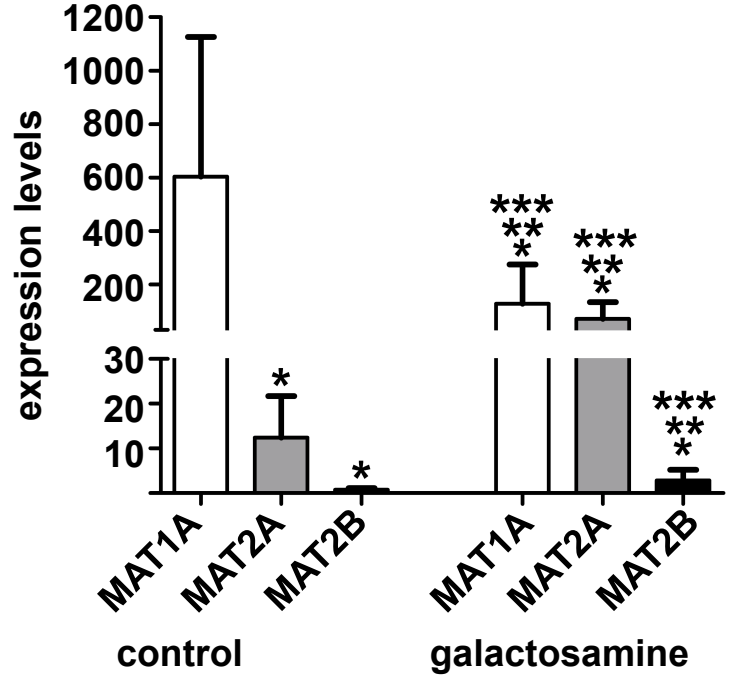
expression levels
1200
1000
800
600
400
200
30
20
10
MAT1A
MAT2A
MAT2B
MAT1A
MAT2A
MAT2B
control
galactosamine

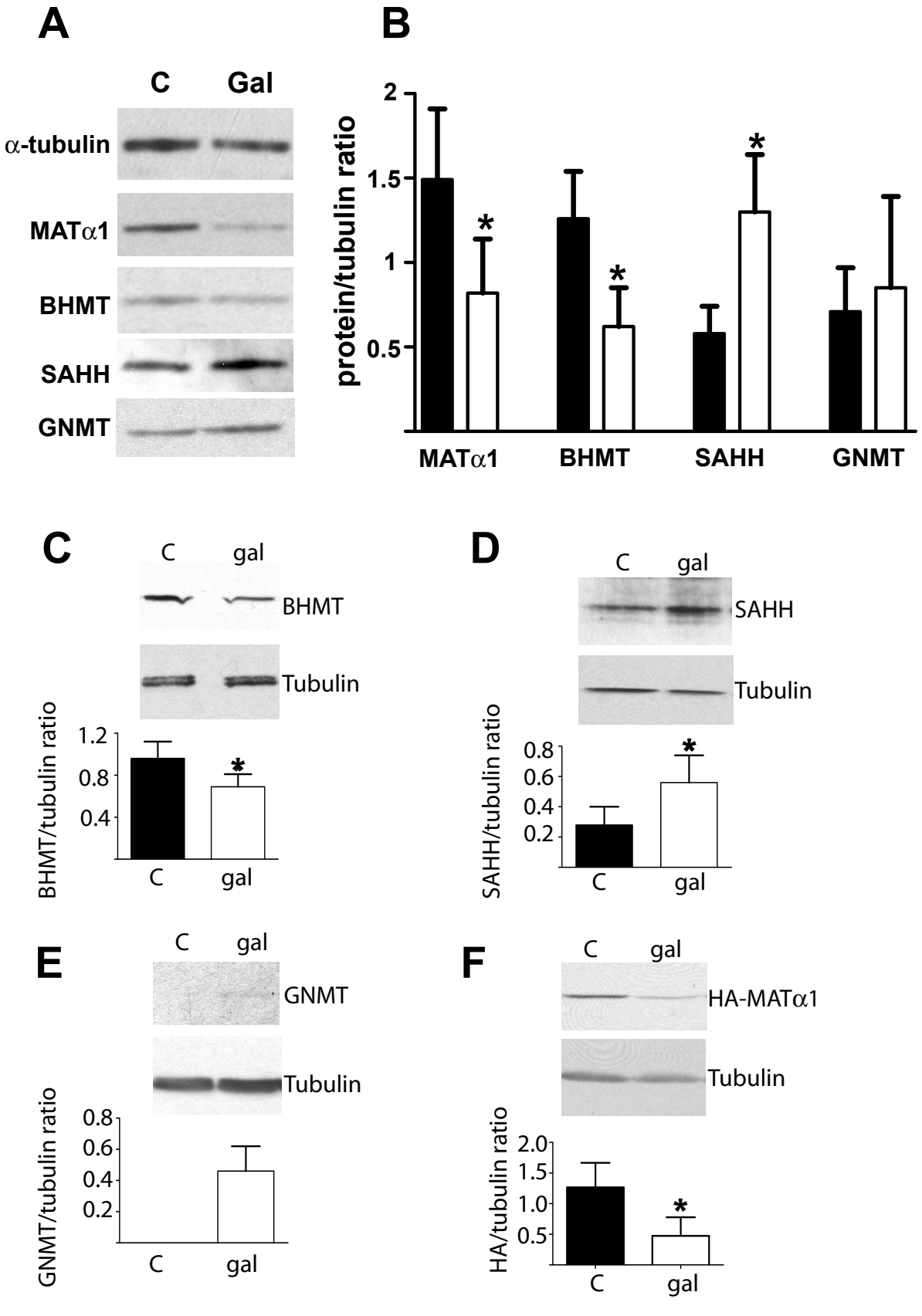
A
C
Gal
α-tubulin
MATα1
BHMT
SAHH
GNMT
B
protein/tubulin ratio
2
1.5
1
0.5
*
*
*
MATα1
BHMT
SAHH
GNMT
C
C
gal
BHMT
Tubulin
BHMT/tubulin ratio
1.2
0.8
0.4
*
C
gal
D
C
gal
SAHH
Tubulin
SAHH/tubulin ratio
0.8
0.6
0.4
0.2
*
C
gal
E
C
gal
GNMT
Tubulin
GNMT/tubulin ratio
0.8
0.6
0.4
0.2
C
gal
F
C
gal
HA-MATα1
Tubulin
HA/tubulin ratio
2.0
1.5
1.0
0.5
*
C
gal

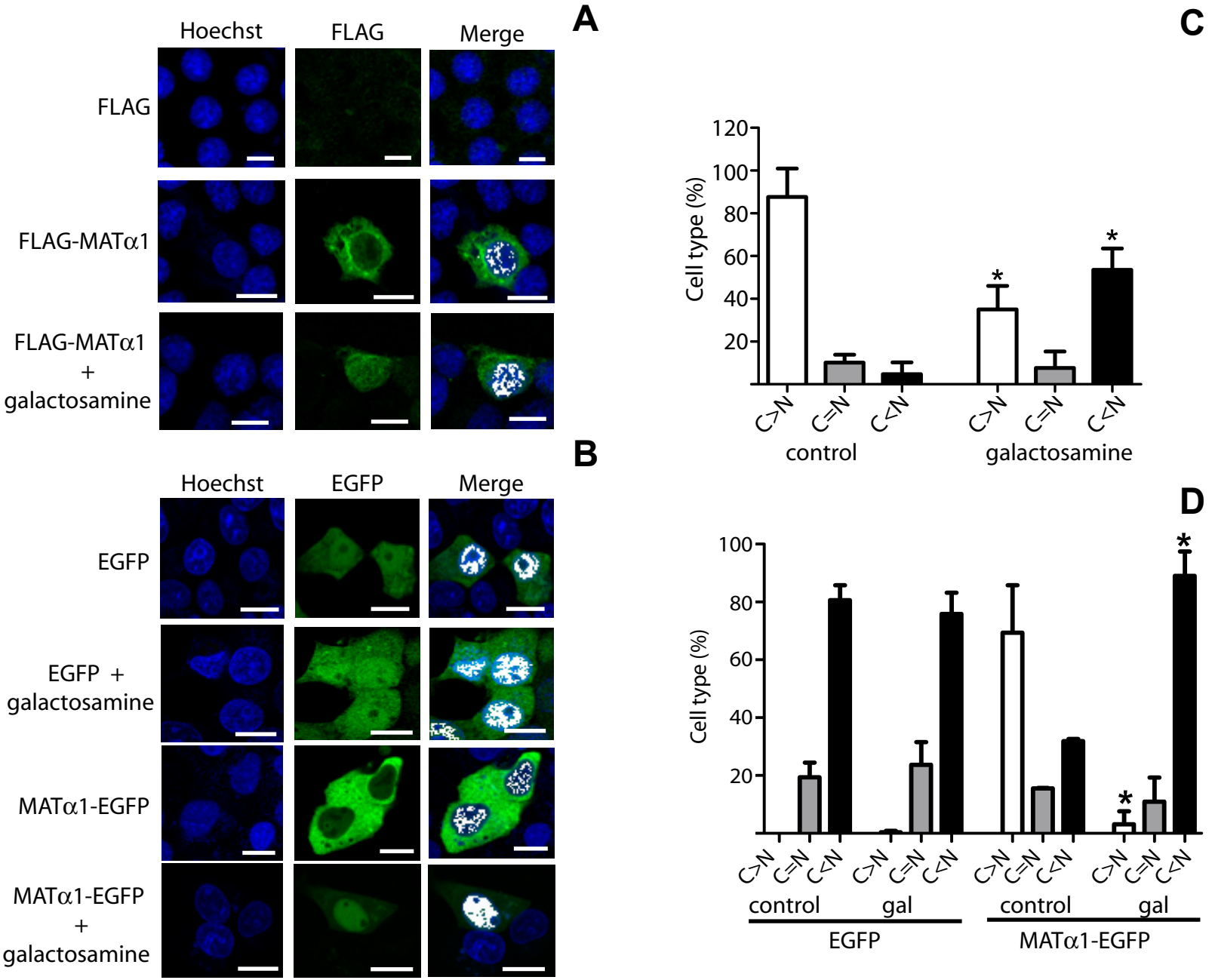
A
Hoechst
FLAG
Merge
FLAG
FLAG-MATα1
FLAG-MATα1
+
galactosamine
B
Hoechst
EGFP
Merge
EGFP
EGFP +
galactosamine
MATα1-EGFP
MATα1-EGFP
+
galactosamine
C
Cell type (%)
120
100
80
60
40
20
C>N
C=N
C<N
control
galactosamine
D
Cell type (%)
100
80
60
40
20
control
gal
EGFP
MATα1-EGFP

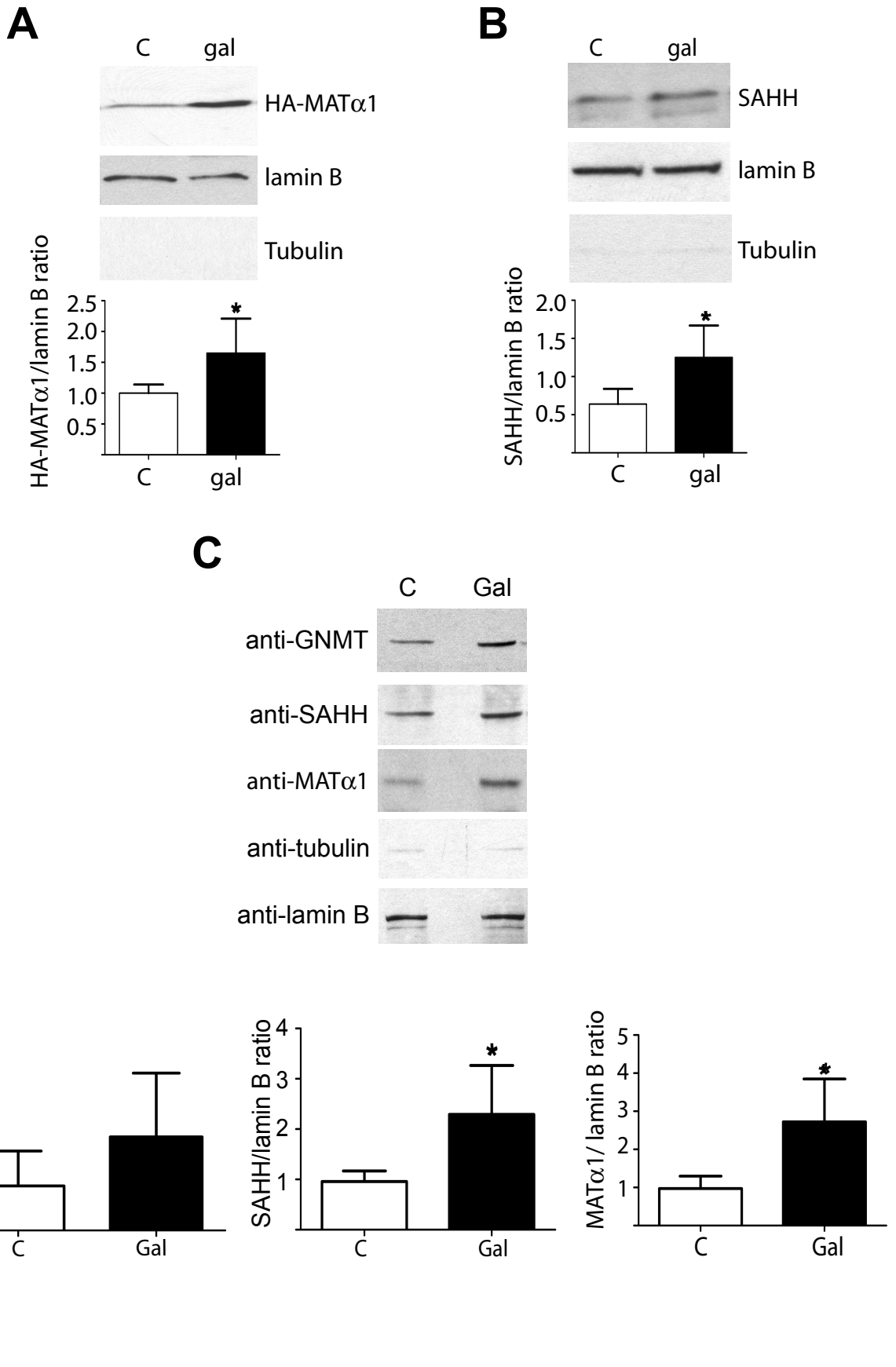
A
C
gal
HA-MATα1
lamin B
Tubulin
HA-MATα1/lamin B ratio
2.5
2.0
1.5
1.0
0.5
*
C
gal
B
C
gal
SAHH
lamin B
Tubulin
SAHH/lamin B ratio
2.0
1.5
1.0
0.5
*
C
gal
C
C
Gal
anti-GNMT
anti-SAHH
anti-MATα1
anti-tubulin
anti-lamin B
D
GNMT/laminB ratio
5
4
3
2
1
C
Gal
SAHH/lamin B ratio
4
3
2
1
*
C
Gal
MATα1/ lamin B ratio
5
4
3
2
1
*
C
Gal

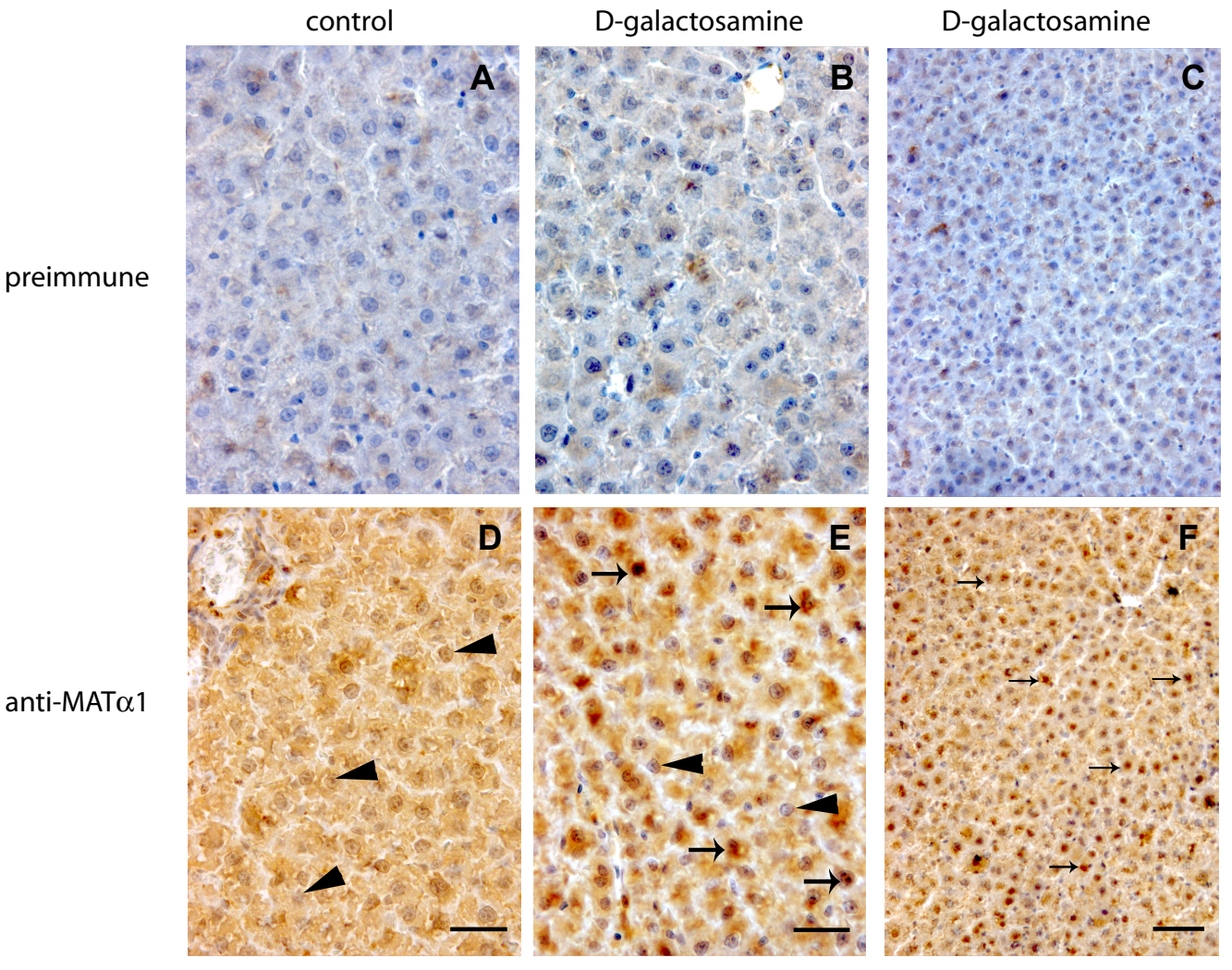
control
D-galactosamine
D-galactosamine
preimmune
anti-MATα1
A
B
C
D
E
F

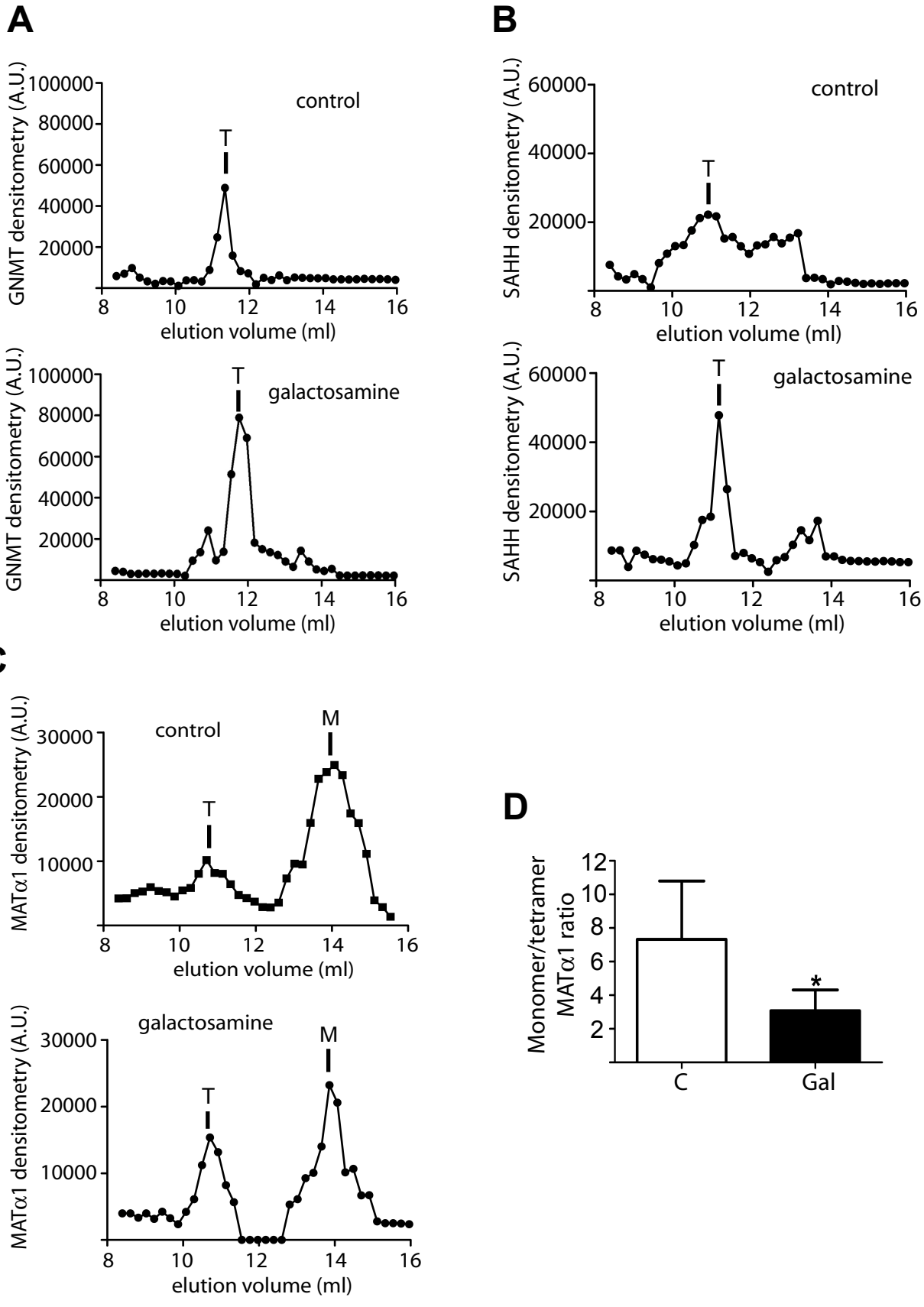
A
GNMT densitometry (A.U.)
100000
80000
60000
40000
20000
control
T
8
10
12
14
16
elution volume (ml)
GNMT densitometry (A.U.)
galactosamine
T
B
SAHH densitometry (A.U.)
60000
40000
20000
control
T
elution volume (ml)
SAHH densitometry (A.U.)
galactosamine
T
C
MATα1 densitometry (A.U.)
30000
20000
10000
control
T
M
elution volume (ml)
galactosamine
D
Monomer/tetramer MATα1 ratio
12
10
8
6
4
2
*
C
Gal

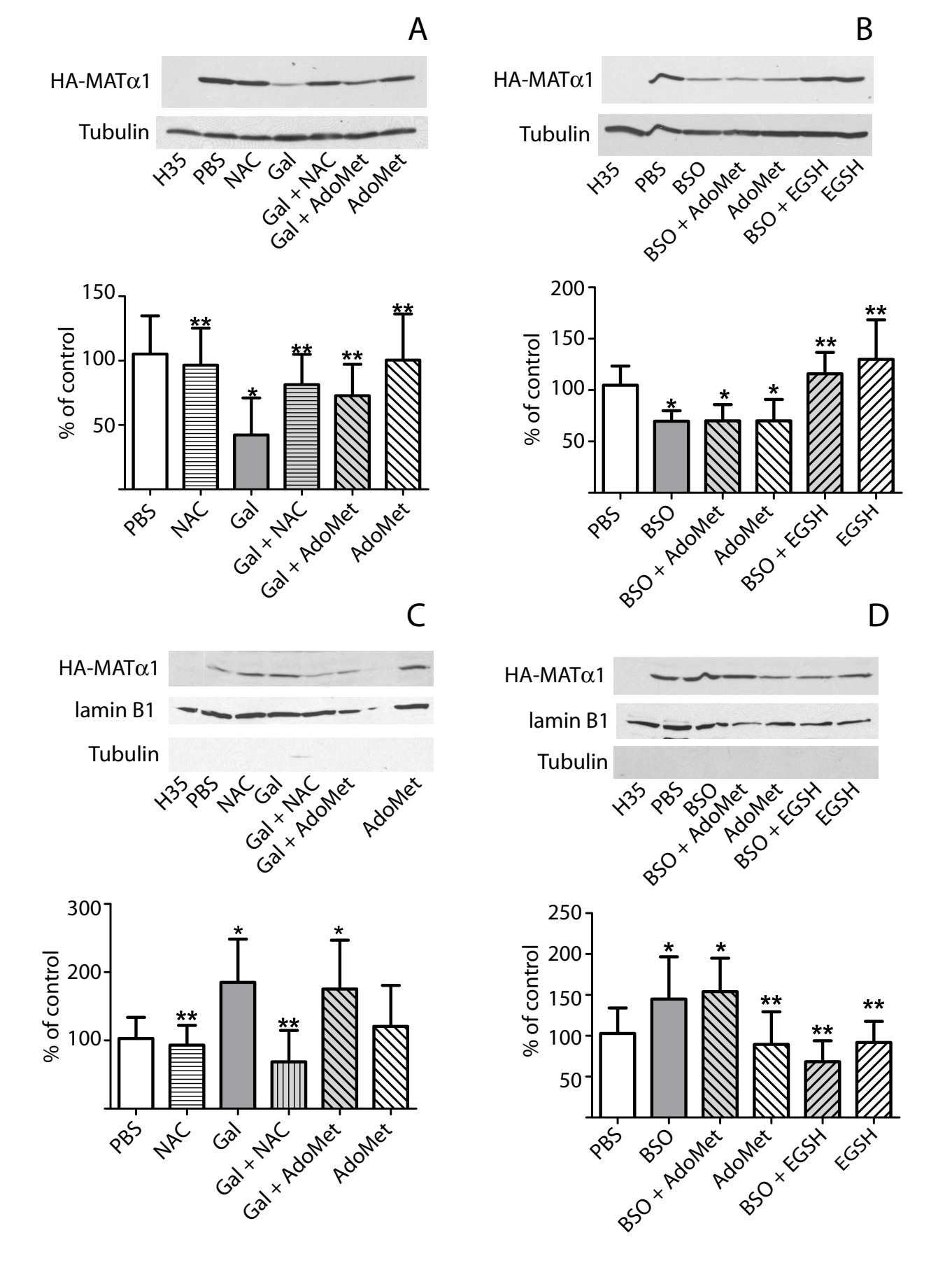
A
HA-MATα1
Tubulin
H35
PBS
NAC
Gal
Gal + NAC
Gal + AdoMet
AdoMet
% of control
150
100
50
PBS
NAC
Gal
Gal + NAC
Gal + AdoMet
AdoMet
B
HA-MATα1
Tubulin
H35
PBS
BSO
BSO + AdoMet
AdoMet
BSO + EGSH
EGSH
% of control
200
150
100
50
PBS
BSO
BSO + AdoMet
AdoMet
BSO + EGSH
EGSH
C
HA-MATα1
lamin B1
Tubulin
H35
PBS
NAC
Gal
Gal + NAC
Gal + AdoMet
AdoMet
% of control
300
200
100
PBS
NAC
Gal
Gal + NAC
Gal + AdoMet
AdoMet
D
HA-MATα1
lamin B1
Tubulin
H35
PBS
BSO
BSO + AdoMet
AdoMet
BSO + EGSH
EGSH
% of control
250
200
150
100
50
PBS
BSO
BSO + AdoMet
AdoMet
BSO + EGSH
EGSH

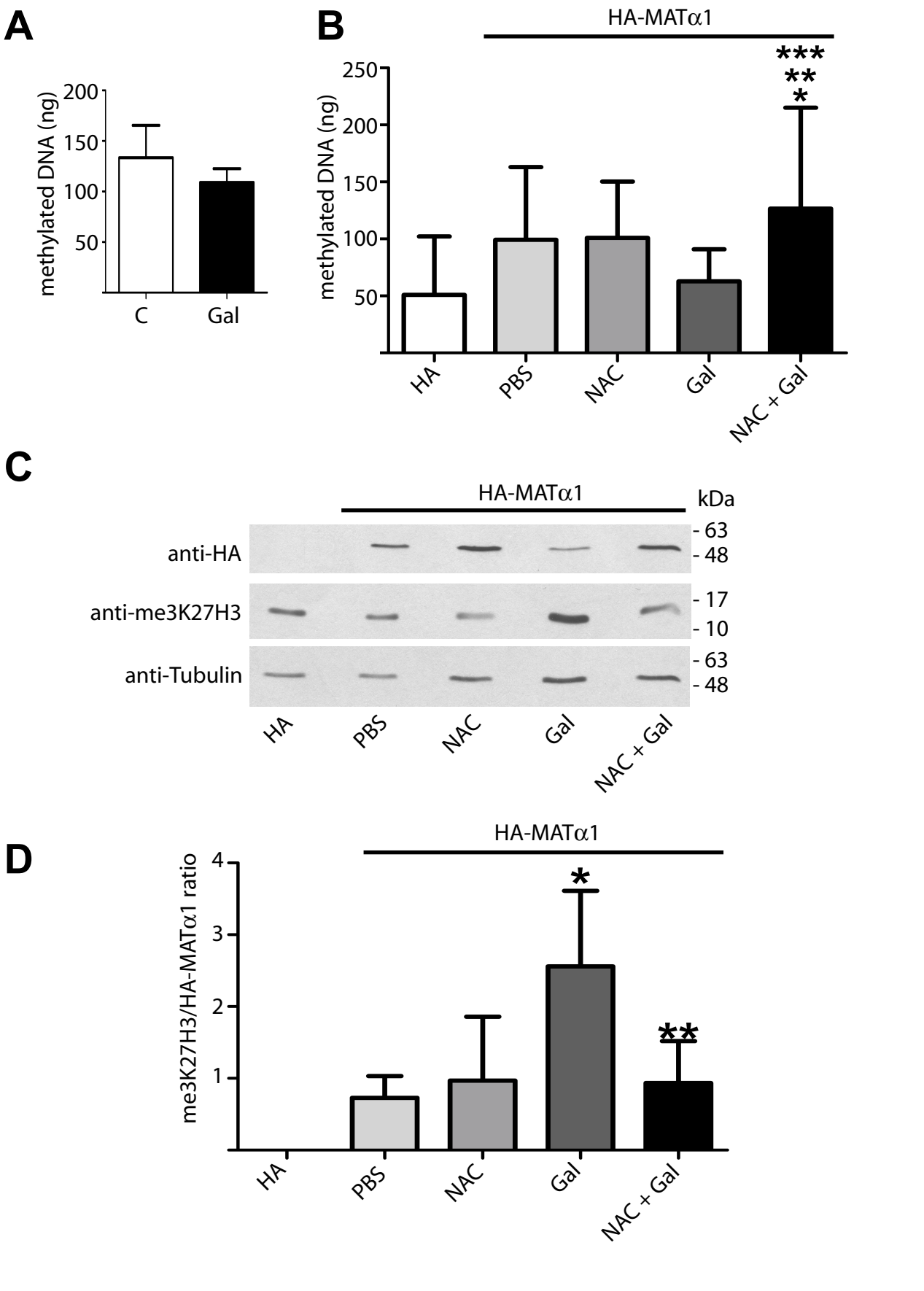
A
methylated DNA (ng)
200
150
100
50
C
Gal
B
HA-MATα1
methylated DNA (ng)
250
200
150
100
50
***
**
*
HA
PBS
NAC
Gal
NAC + Gal
C
HA-MATα1
kDa
anti-HA
anti-me3K27H3
anti-Tubulin
- 63
- 48
- 17
- 10
- 63
- 48
HA
PBS
NAC
Gal
NAC + Gal
D
HA-MATα1
me3K27H3/HA-MATα1 ratio
4
3
2
1
*
**
HA
PBS
NAC
Gal
NAC + Gal

Supplementary information

ACUTE LIVER INJURY INDUCES NUCLEOCYTOPLASMIC REDISTRIBUTION OF HEPATIC METHIONINE METABOLISM ENZYMES

Miguel Delgado, Francisco Garrido, Juliana Pérez-Miguelsanz, María Pacheco, Teresa Partearroyo, Dolores Pérez-Sala and María A. Pajares

INDEX OF CONTENTS

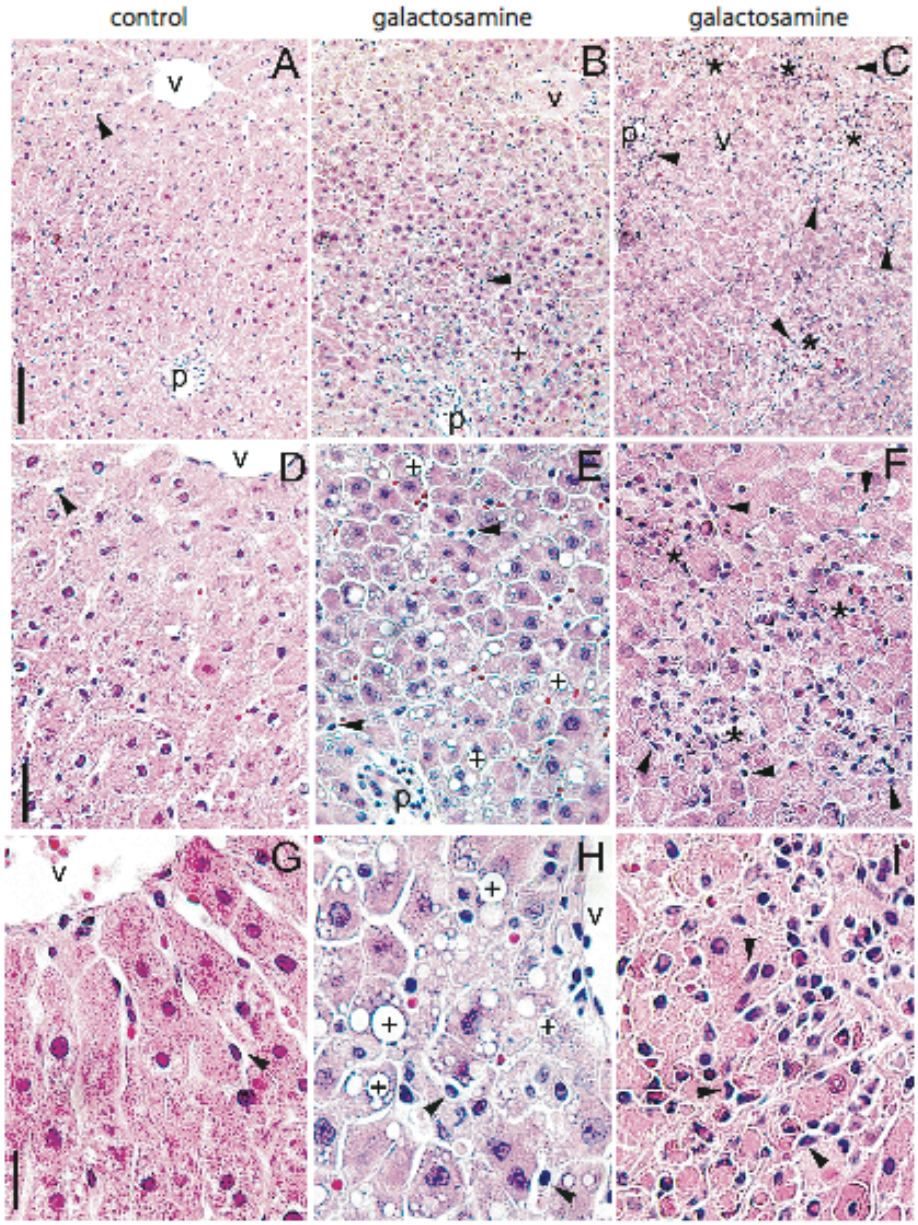

Supplementary FIG. S1. Histological evaluation of the livers of control and D-galactosamine-treated rats. Paraffin embedded sections of livers from control (A, D,G) and galactosamine–treated animals (B, C, E, F, H, I) were prepared for hematoxylin-eosin staining. The figure shows representative panels for individuals in each group, proving the presence of acute liver injury in the treated animals. Focal necrosis (∗), Kupffer cell hyperplasia and inflammatory cell infiltration (arrowheads) were visible. In one case, fat infiltration (+) in the periportal area was also observed (B, E, H). Locations of portal vessels (p) and central vein (v) are also indicated. The bar scale corresponds to 50 μm (A-C), 20 μm (D-F) and 10 μm (G-I).

Supplementary Table S1

Activity measurements. Alanine aminotransferase (ALT) and aspartate aminotransferase (AST) activities were measured in serum, whereas MAT and BHMT activities were determined in liver cytosol from control and D-galactosamine-treated animals receiving two 400 mg/kg i.p. doses of the agent as described under Materials and Methods. The assay conditions correspond to: total MAT activity (5 mM methionine); MAT I and MAT II activities (60 μM methionine); and MAT I, MAT II and stimulated MAT III activities (60 μM methionine plus 10% v/v DMSO). Activity in MATα1 tetramer (MAT I) and dimer (MAT III) peaks obtained by AGFC was measured at saturating concentrations of the substrates to calculate the MAT I/III activity ratio for animals in each group. The data shown are the mean ± SD of measurements made in triplicate for every individual in each group.

	Assay conditions	**control (n=15)**	**galactosamine (n=16)**	**p value**
ALT (U/l)	serum	28.33 ± 3.41	1212 ± 454.2*	<0.001
AST (U/l)	serum	131.5 ± 22.32	2466.0 ± 749.8*	<0.001
MAT (pmol/min/mg)	60 μM Met	50.33 ± 3.43	54.03 ± 3.17	0.51
	60 μM Met + 10% DMSO	503.34 ± 34.27	622.31 ± 51.49	0.17
	5 mM Met	689.0 ± 132.2	336.1 ± 43.57*	0.04
BHMT (nmol/min/mg)	6.5 mM Betaine + 6.5 mM Hcy	0.268 ± 0.05	0.197 ± 0.07*	0.02
MAT III/I ratio	5 mM Met	1.08 ± 0.11	1.45 ± 0.56	0.29†

*significant, p≤ 0.05.

†variances significantly different according to Bartlett's test

Supplementary Table S2

Hepatic metabolite levels determined by UPLC-MS in liver samples of the galactosamine model.

	Control† (n=12)	Galactosamine† (n=10)	p value
AdoMet (nmol/g)	71.38 ± 14.32	47.98 ± 9.21*	0.03
AdoHcy (nmol/g)	51.54 ± 10.84	44.88 ± 9.34	0.37
AdoMet/AdoHcy	1.50 ± 0.19	1.07 ± 0.17*	0.03
Hcy (nmol/g)	5.34 ± 0.51	6.72 ± 0.97*	0.01
Methionine (nmol/g)	180.4 ± 42.64	265.3 ± 62.24*	0.03
GSH (nmol/mg protein)	85.67 ± 26.5	122.0 ± 29.88	0.09
GSSG (nmol/mg protein)	2.07 ± 0.81	3.99 ± 1.67*	0.04
GSH/GSSG	43.60 ± 6.13	29.88 ± 10.68*	0.03

*significant, p≤ 0.05.

† The results are the amount quantified per gram of tissue for each group (mean ± SD).

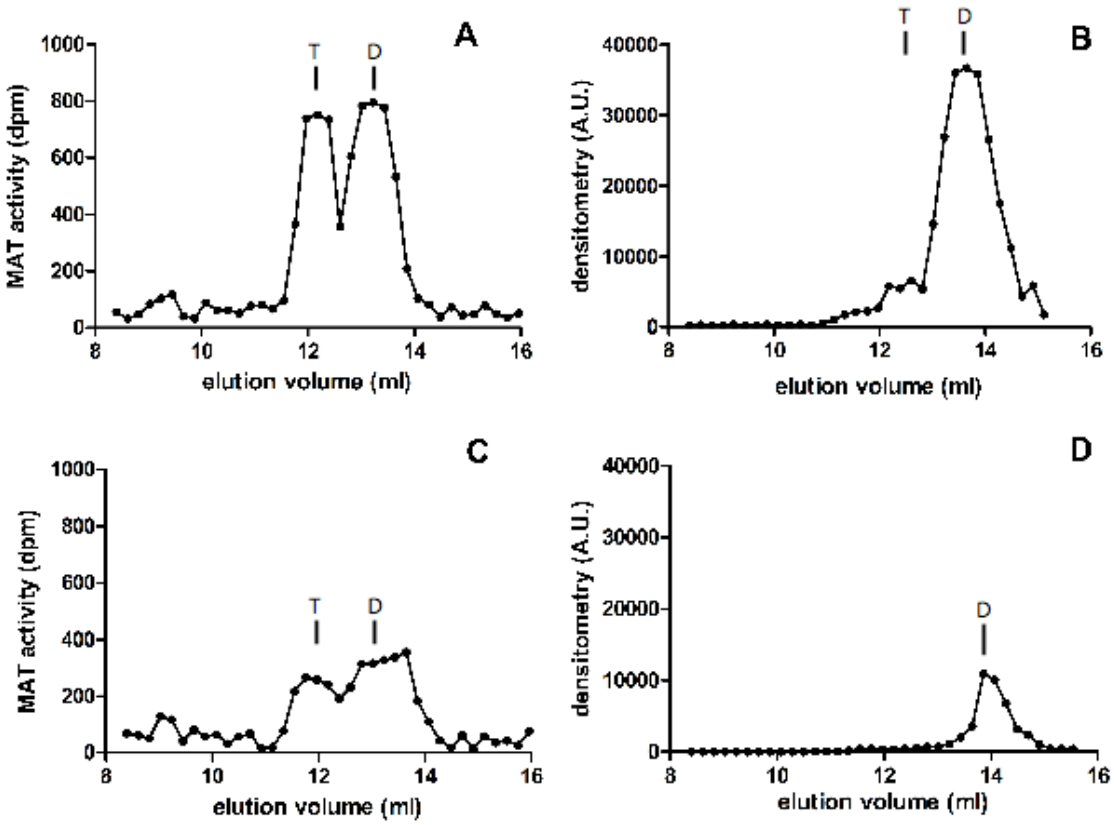

Supplementary FIG. S2. Gel filtration chromatography profiles of cytosolic MAT I/III. Cytosolic samples (1 mg) of control (A and B) and D-galactosamine-treated rat livers (C and D) were loaded on a Superose 12/10 HR column and the eluting fractions collected. Samples of these fractions were used to measure total MAT activity at 5 mM methionine (A and C), and for dot-blot analysis of MATα1 protein (B and D). The figure shows profiles of representative samples of each group. The markers eluted as follows: blue dextran (7.66 ml), apoferritin (9.87 ml), β-amylase (11.97 ml), alcohol dehydrogenase (12.81 ml), carbonic anhydrase (15.12 ml) and ATP (19.26 ml). The elution volumes for tetramers (T) and dimers (D) are indicated.

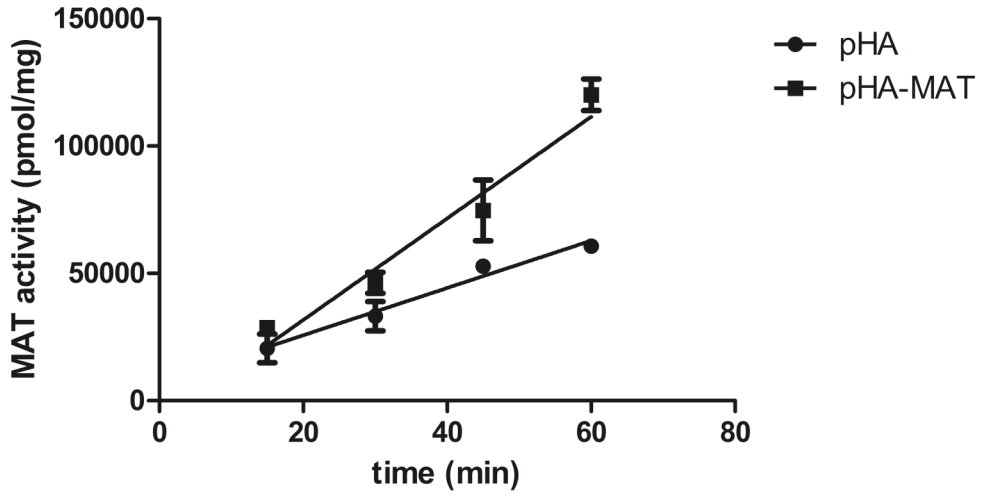

Supplementary FIG. S3. HA-MATα1 activity as a function of time. HA-MATα1 was overexpressed in *E. coli* BL21(DE3) cells and the soluble fraction isolated. MAT activity was measured using a reaction mixture containing 5 mM methionine and 5 mM ATP. The reaction was carried out in triplicate at 37ºC and the production of AdoMet analyzed at 15, 30, 45 and 60 min. The same analysis was carried out in parallel using pHA transformed cells, in order to determine the background provided by the *E. coli* MAT isoenzyme. The figure shows results (mean ± SD) of a representative experiment carried out in triplicate. Calculated specific activities were determined for pHA (928.2 ± 79.15 pmol/min/mg) and pHA-MAT (1995.0 ± 220.7 pmol/min/mg) transformed cells.

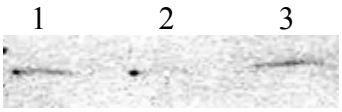

Supplementary FIG. S4. HA-MATα1 levels in the soluble fraction of BL21(DE3) cells. The figure shows a representative western blot of samples from the soluble fraction (lane 1), a 1:10 (v/v) dilution of this fraction (lane 2) and a concentrated sample of the HA-MATα1 peak eluted from analytical gel filtration chromatography (lane 3) using anti-HA. HA-MATα1 exhibits a calculated molecular mass of 53.8 kDa according to the mobility of the standards. The low expression observed in the soluble fraction can explain the low level of activity detected.

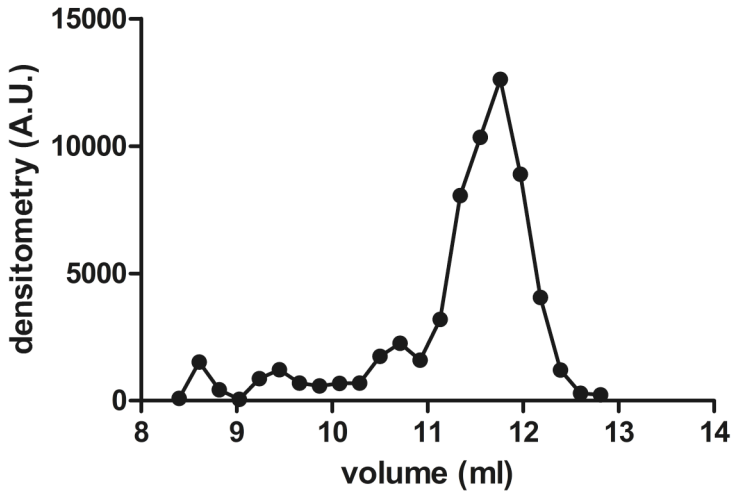

Supplementary FIG. S5. Analytical gel filtration chromatography elution profile of HA-MATα1. A sample of the soluble fraction (100 μl) obtained from *E. coli* BL21(DE3) transfected with pHA-MAT was injected onto a Superose 12 10/300 GL gel filtration chromatography column and run at 0.3 ml/min. Fractions (210 μl) were collected and aliquots (100 μl) were used for Dot-Blot detection of HA-MATα1 using anti-HA. The intensity of the spots was established by densitometric scanning using ImageJ software and represented against the elution volume. The figure shows a representative elution profile of three experiments carried out in triplicate. The elution volume of the markers was as follows: blue dextran (7.13 ml), apoferritin (9.55 ml), β-amylase (10.38 ml), alcohol dehydrogenase (11.05 ml), carbonic anhydrase (13 ml) and ATP (17.39 ml). The elution volume of the main peak detected corresponds to that expected for a protein of ~85 kDa, in agreement with that estimated for a dimer of HA-MATα1 subunits.

Supplementary Table S3

Effect of D-galactosamine treatment on mRNA and protein half-lives in H35 cells. H35 hepatoma cells were treated with 10 mM D-galactosamine for 48 hours before addition of 5 μg/ml actinomycin D (†) or 20 μg/ml cycloheximide (¶) in the absence of serum to determine mRNA or protein half-lives, respectively. The results shown are the average of three experiments carried out in triplicate (mean ± SD) and were considered significant when p≤ 0.05 (*).

	mRNA half-life (hours)†		
	Control§	**Galactosamine§**	**p value**
MAT2A	5.83 ± 2.44	6.25 ± 1.78	0.79
MAT2B	6.76 ± 1.90	12.53 ± 2.44*	0.02
SAHH	67.36 ± 29.88	9.77 ± 0.70*	0.02
MTR	12.48 ± 4.16	13.49 ± 10.22	0.86
BHMT	82.53 ± 77.0	9.58 ± 10.14	0.24
GCLl	4.00 ± 0.56	7.70 ± 2.06*	0.02
GCLm	11.23 ± 4.82	39.80 ± 1.88*	0.003
	Protein half-life (hours)¶		
BHMT	16.34 ± 6.25	44.20 ± 20.47*	0.05
SAHH	14.62 ± 3.22	34.85 ± 15.27*	0.01

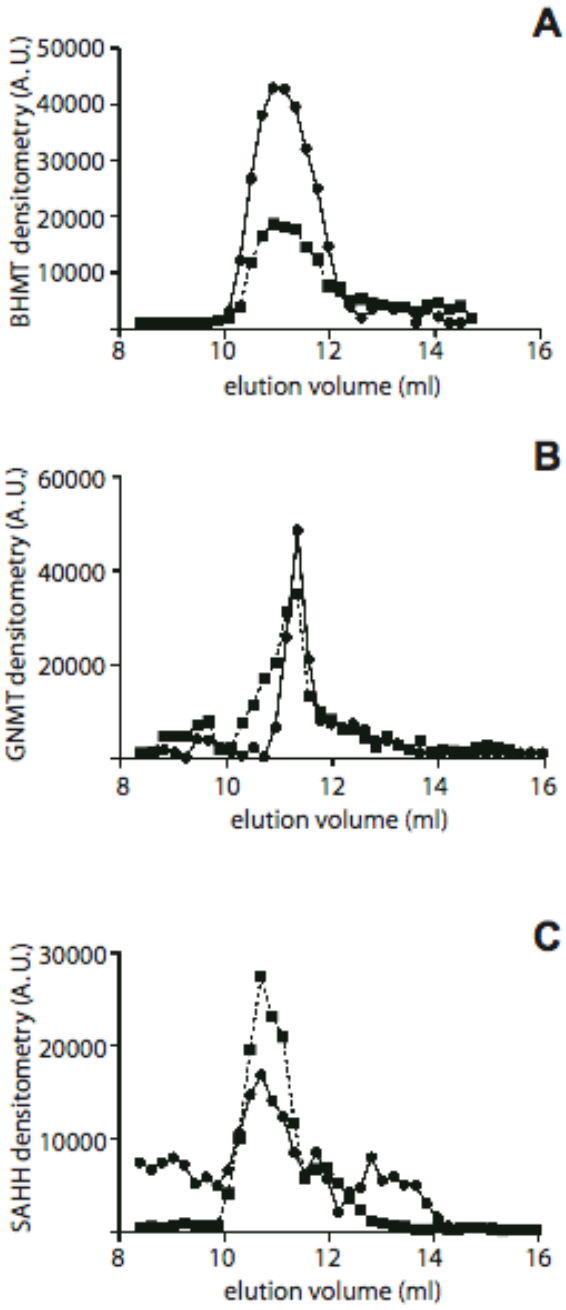

Supplementary FIG. S6. Analytical gel filtration chromatography profiles of cytosolic BHMT, GNMT and SAHH. Liver cytosols (100 μl) from control (●) and galactosamine-treated (■) animals were injected onto a Superose 12 10/300 GL gel filtration chromatography column and run at 0.3 ml/min. Fractions (210 μl) were collected and aliquots (50 μl) were used for Dot-Blot detection of BHMT (panel A), GNMT (panel B) or SAHH (panel C) using the corresponding antibodies. The intensity of the spots was established by densitometric scanning using ImageJ software and represented against the elution volume. The figure shows a representative elution profile of six independent experiments carried out in duplicate. The elution volume of the markers was as follows: blue dextran (7.13 ml), apoferritin (9.55 ml), β-amylase (10.38 ml), alcohol dehydrogenase (11.05 ml), carbonic anhydrase (13 ml) and ATP (17.39 ml).

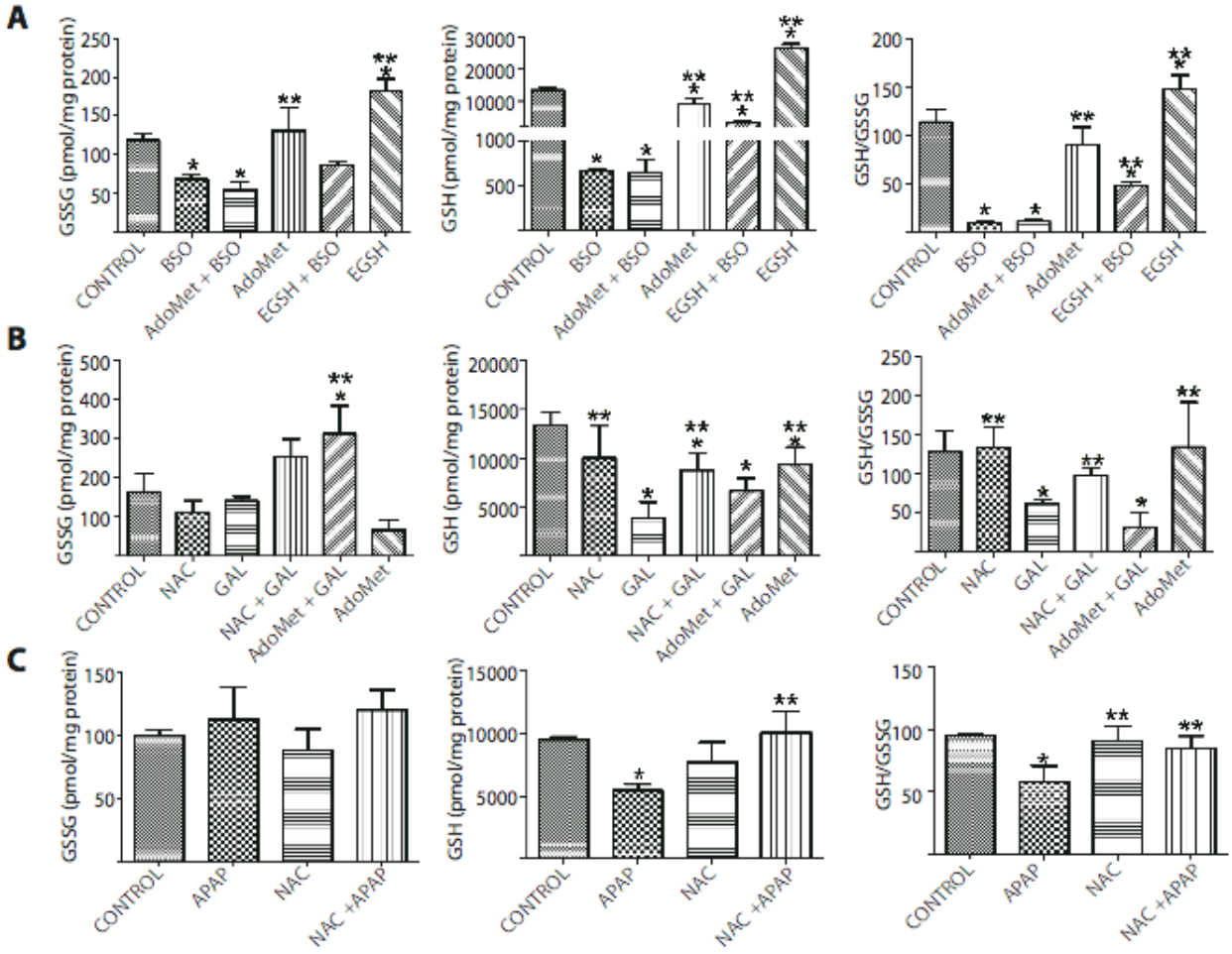

Supplementary FIG. S7. Glutathione levels in transfected H35 cells subjected to different treatments. GSH and GSSG levels were determined in transfected H35 cells after the addition of 1 mM BSO (panel A), 10 mM galactosamine (Gal; panel B) or 5 mM acetaminophen (APAP; panel C) alone or in combination with 5 mM N-acetylcysteine (NAC), 1 mM glutathione ethyl ester (EGSH) or 0.5 mM AdoMet. Appropriate controls including the vehicle (PBS or 1% ethanol) were included for comparison. Left panels show calculated GSSG levels, central panels depict the GSH content and right panels represent the calculated GSH/GSSG ratio. The results shown are the mean ± SD of four independent experiments carried out in triplicate.

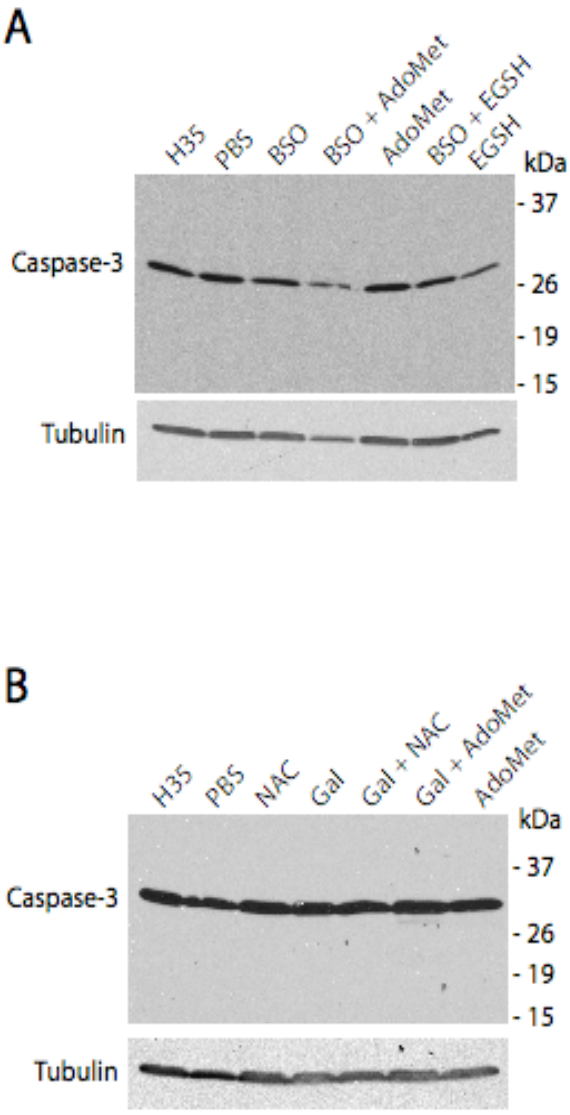

Supplementary FIG. S8. Effects of buthionine sulfoximine and D-galactosamine treatments on caspase-3 activation in pHA-MAT transfected cells. Hepatoma H35 cells transiently transfected with pHA-MAT were treated with buthionine sulfoximine (BSO) for 24 h alone or in combination with AdoMet or EGSH (panel A). Transfected cells were also treated for 48 h with galactosamine (Gal) alone or in combination with AdoMet or NAC (panel B). Cellular extracts were obtained and samples (50 μg) were analyzed by western blot using anti-caspase-3 and anti-tubulin antibodies. Representative western blots of nine independent experiments are shown in the figure. The mobility and size of the standards is indicated on the right.

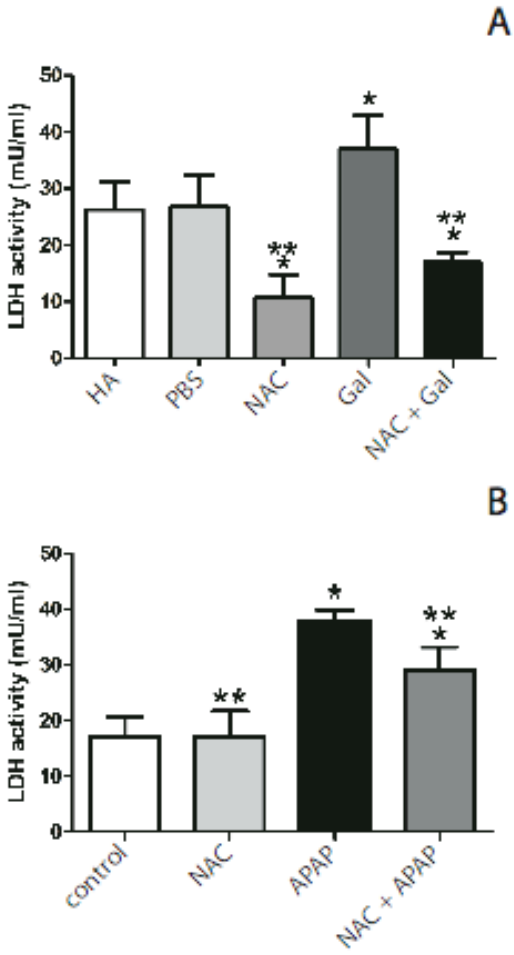

Supplementary FIG. S9. LDH activity measured in the culture media of H35 cells transfected with pHA-MAT. H35 transfected cells were treated with 10 mM galactosamine (Gal; 48 hours), 5 mM acetaminophen (APAP; 24 hours), 5 mM N-acetylcysteine (NAC) or their combinations. LDH activity was measured in the cell media (100 μl). The figure shows results (mean ± SD) of six independent experiments carried out in triplicate for galactosamine (panel A) and acetaminophen treatments (panel B). Multiple comparisons of the data were carried out with ANOVA using GraphPad Prism and considered significant when p≤ 0.05 vs. PBS (*), Gal or APAP (**).

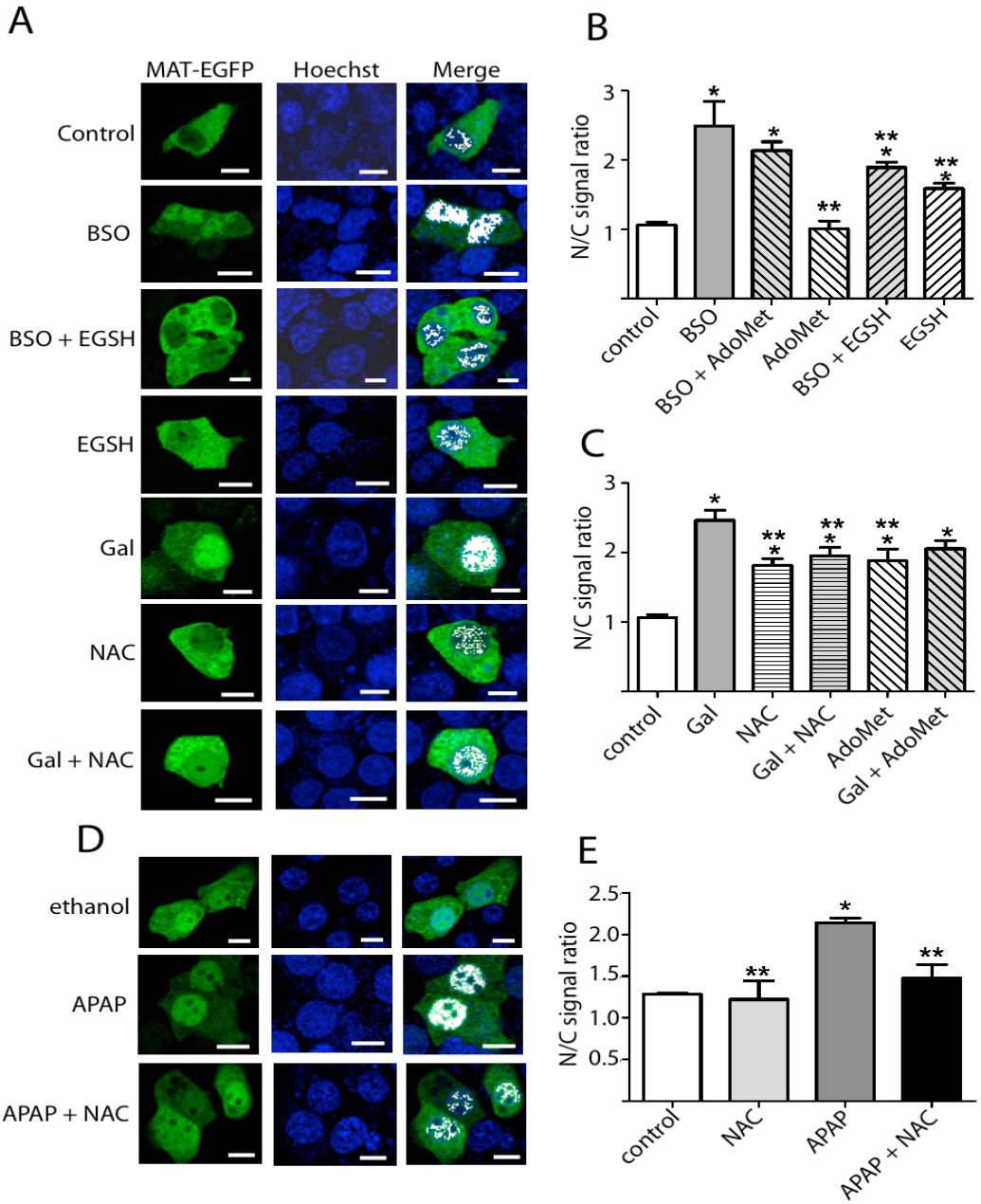

Supplementary FIG. S10. Effects of redox-modulating agents on nucleocytoplamic distribution of MATα1-EGFP analyzed by in vivo confocal microscopy. Hepatoma H35 cells were transiently transfected with pMAT-EGFP and the effect of several additives analyzed in vivo by confocal microscopy. Panels A and D show representative confocal images of several treatments, including colocalization with nuclear staining (bar scale=10 μm). Nuclear (N) and cytoplasmic (C) EGFP signals were quantified using the Leica Confocal Software and the N/C ratio calculated for a minimum of 100 cells per treatment. Panel B depicts quantification results obtained in experiments with BSO (24h); panel C shows data of D-galactosamine (48h) treatments; and panel E illustrates quantifications obtained in experiments including acetaminophen (24h). For graphical purposes panels B, C and E depict the mean ± SEM of the data analyzed using ANOVA with Bonferroni post-hoc testing. Significant changes ($p \leq 0.05$) vs. control with PBS or ethanol (*), and BSO, galactosamine or acetaminophen (**) are indicated.

Supplementary Table S4

Activities and metabolite levels in rats treated with acetaminophen. Alanine aminotransferase (ALT) and aspartate aminotransferase activities were measured in serum samples of control and acetaminophen treated animals. On the other hand, metabolite levels and cytosolic MAT activity were determined in liver samples as described under Materials and Methods. The activity data shown are the mean ± SD of measurements made in triplicate for every individual in each group.

	Assay conditions	control (n=6)	acetaminophen (n=6)	p value
ALT (U/l)	Serum	28.33 ± 3.41	1324 ± 453*	<0.0001
AST (U/l)	serum	131.5 ± 22.32	2630 ± 1075.8*	<0.0001
AdoMet (nmol/g)	liver	77.43± 8.20	59.43 ± 5.05*	0.049
AdoHcy (nmol/g)	liver	48.79 ± 5.33	30.82 ± 3.49*	0.045
AdoMet/AdoHcy	liver	1.42 ± 0.08	2.33 ± 0.27*	0.001
Hcy (nmol/g) †	liver	<1.5	<1.5	-
Methionine (nmol/g)	liver	186.6 ± 38.90	94.88 ± 18.54*	0.012
GSH (nmol/mg protein)	liver	77.31 ± 20.48	41.45 ± 10.37*	0.04
GSSG (nmol/mg protein)	liver	1.58 ± 0.04	1.15 ± 0.05*	0.001
GSH/GSSG	liver	47.87 ± 3.06	36.34 ± 6.28*	0.049
MAT (pmol/min/mg)	60 µM Met	161.5 ± 4.39	128.0 ± 4.91*	0.001
	60 µM Met + 10% DMSO	654.8 ± 25.21	611.4 ± 14.93	0.195
	5 mM Met	2389.0 ± 131.1	1957.0 ± 121.7*	0.027
MAT III/I activity ratio	5 mM Met	1.08 ± 0.11	2.35 ± 0.70*	0.016

*significant, p≤ 0.05.

†below the quantification limit

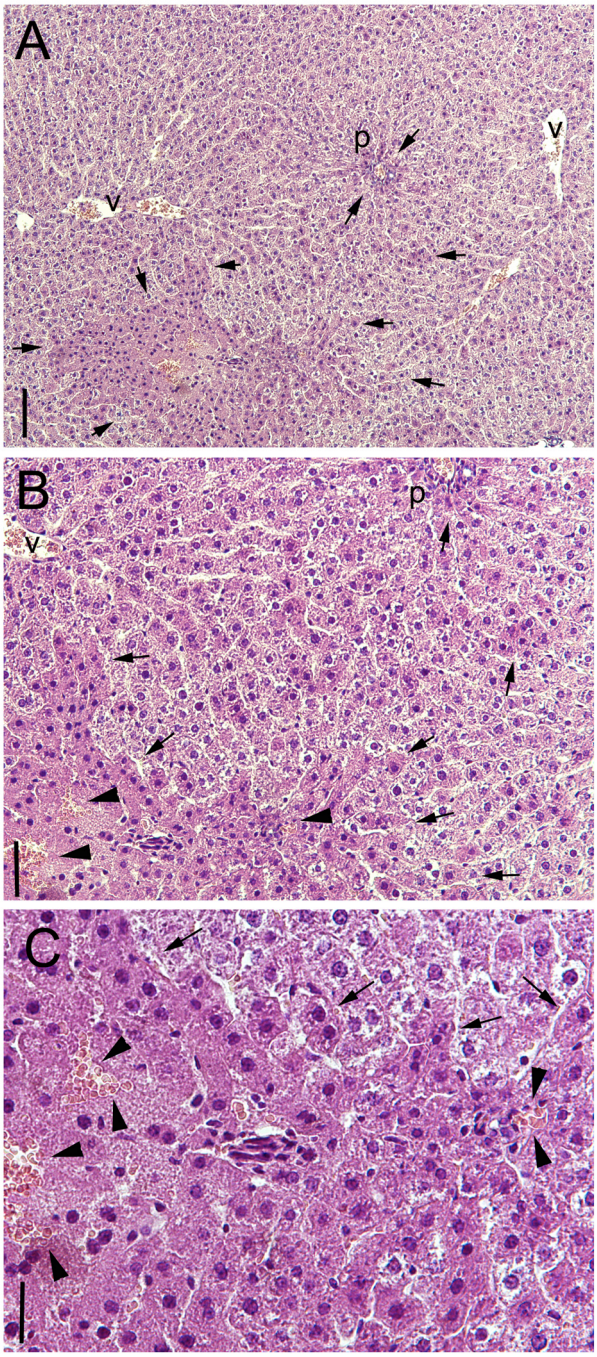

Supplementary FIG. S11. Histological evaluation of liver sections of rats treated with acetaminophen. Paraffin embedded sections of livers from acetaminophen–treated animals were prepared for hematoxylin-eosin staining. The figure shows representative photomicrographs proving the presence of a large number of necrotic hepatocytes (arrows). The presence of sinusoidal congestion with red blood cells (arrowheads) was visible as compared to the normal architecture of control liver sections (Supplementary Fig. 1, panels A,D,G). The bar scale corresponds to 100 μm (A), 50 μm (B) and 10 μm (C).

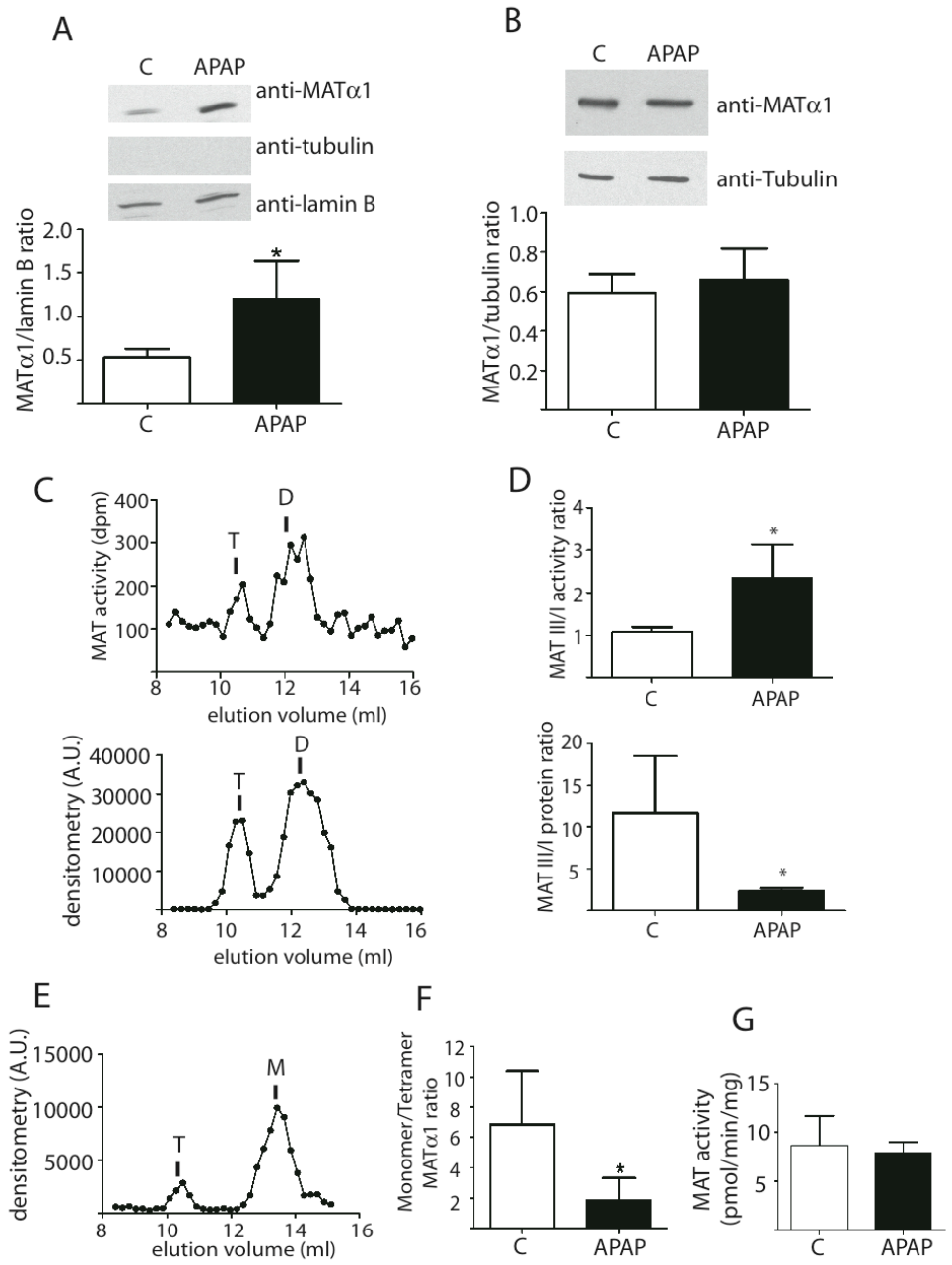

Supplementary FIG. S12. Effects of acetaminophen treatment on MATα1 subcellular distribution and oligomerization in rat liver. Cytosolic and nuclear fractions were isolated from livers of control and acetaminophen-treated rats. Panel A shows MATα1 levels in nuclear fractions using lamin B as the reference, whereas panel B illustrates MATα1 levels in the cytosol using α-tubulin as the loading control. Representative MAT activity and dot-blot profiles (n=6) of cytosolic samples analyzed on a Superose 12 10/300 GL gel filtration chromatography column run at 0.3 ml/min are depicted in panel C, whereas a representative dot-blot profile of a nuclear sample appears in panel E. The elution volume of the markers was as follows: blue dextran (7.13 ml), apoferritin (9.55 ml), β-amylase (10.38 ml), alcohol dehydrogenase (11.05 ml), carbonic anhydrase (13 ml) and ATP (17.39 ml). Quantification of the cytosolic dimer/tetramer activity and protein ratios are shown in panel D, whereas the nuclear monomer/tetramer ratio appears in panel F. Panel G illustrates nuclear MAT activity in control and acetaminophen-treated livers. The results shown are the mean ± SD of six independent samples; $p \leq 0.05$ (*).

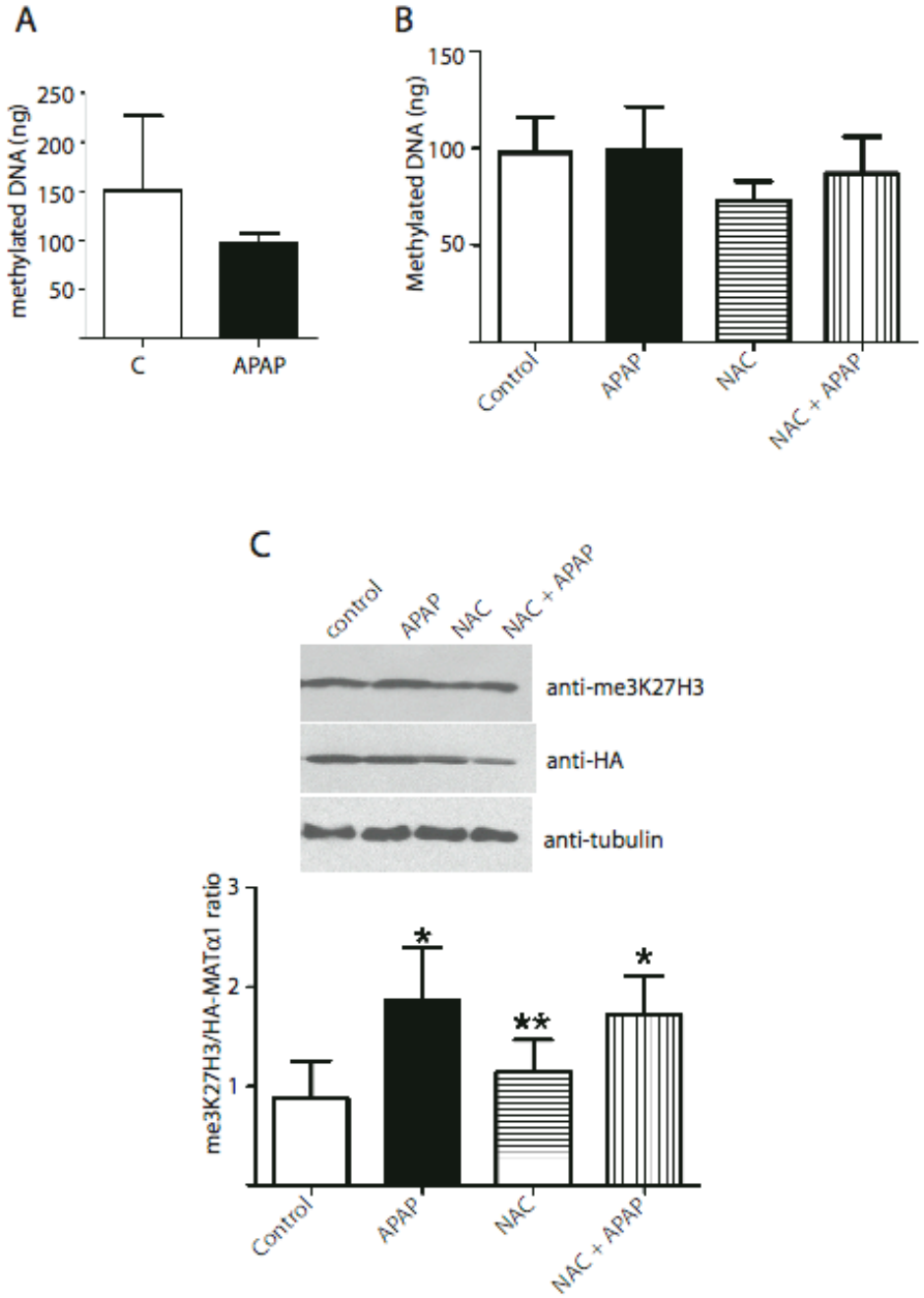

Supplementary FIG. S13. Effects of acetaminophen on DNA and histone methylations. The figure shows the effects of acetaminophen (APAP) treatment on global DNA methylation in DNA samples of control and acetaminophen treated livers (panel A). In addition, the effects of APAP alone or in combination with NAC were also evaluated in H35 transfected cells. Panel B, depicts the changes in global DNA methylation induced by the treatments in pHA-MAT transfected cells, whereas panel C illustrates the alterations observed in K27 trimethylation of histone 3. The histograms show the mean ± SD of three independent experiments carried out in triplicate. Multiple comparisons were carried out with ANOVA; $p \leq 0.05$ vs. control (*) or APAP (**)

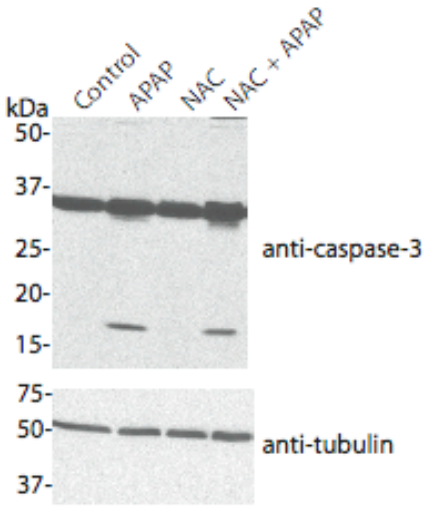

Supplementary FIG. S14. Effects of acetaminophen treatment on caspase-3 activation in pHA-MAT transfected cells. Hepatoma H35 cells transiently transfected with pHA-MAT were treated with acetaminophen (APAP) for 24 h alone or in combination with NAC. Cellular extracts were obtained and samples (50 μg) were analyzed by western blot using anti-caspase-3 and anti-tubulin antibodies. Representative western blots of five independent experiments are shown in the figure. The mobility and size of the standards is indicated on the left.

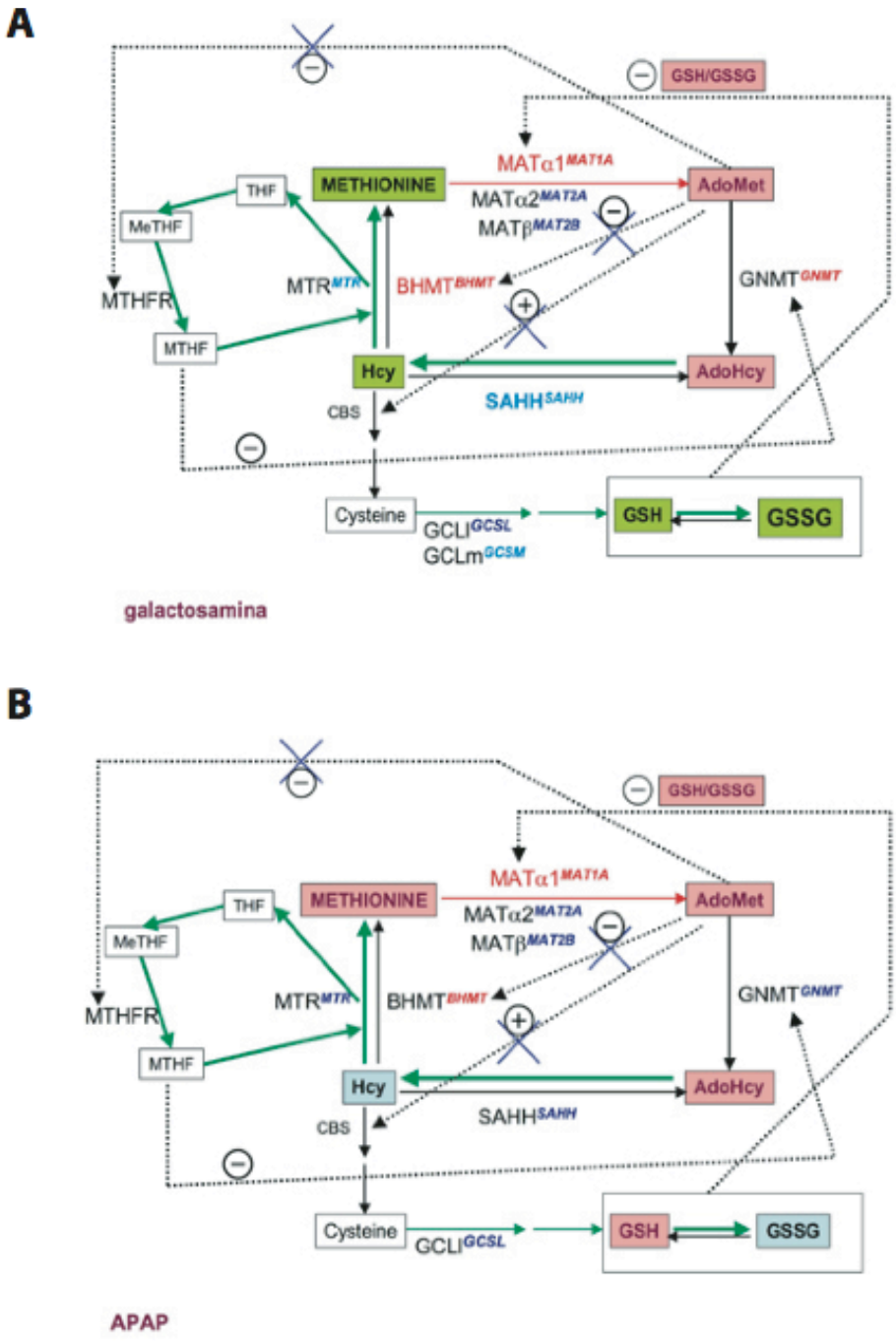

Supplementary FIG. S15. Schematic representation of the cytoplasmic changes in the methionine cycle and connecting pathways detected in the animal models used. (A) Changes in the galactosamine model and (B) alterations detected in the APAP model. Metabolites measured in this study appear in boxes colored according to the changes observed, decreased (red), increased (green) and non-modified levels (light blue). Metabolites that were not determined appear in white boxes. Changes in mRNA levels are indicated as superscripts to the protein symbol, those included in panel B were reported by Schnackenberg et al. (56). Again, a color code has been used to indicate the alterations observed: decrease (red), increase (light blue) and sharp increase (dark blue); black characters indicate no change or undetected protein. Colored arrows indicate the favored (green), decreased (red) or unchanged (black) reactions under according to our results (galactosamine) and/or Schnackenberg et al. (APAP). Nuclear changes in protein levels have been excluded for clarity.

Supplementary Table S5

Primer sequences used for Real Time-PCR experiments designed with Primer Express 3.0.

	Forward (5´-3)	Reverse (5´-3´)	nM*
MAT 1A	GCGAGAGCTACTAGAGGTTGTGAA	AGATCCAAGTCCCTGACAATAACAC	300
MAT 2A	GGAGGGTTCTTGTTCAGGTCTCT	GGAAAATGGAGATCGACAATGG	300
MAT 2B	GCAATTGCAGACGCCTTCA	CAGGGCTGTCAGTAATAGGTCGTA	300
BHMT	GGAGATCTACATGGCGTGTCT	CGGCACCTGCTTTTACCAAA	300
MS	TCTGTGAAGACCTCATCTGGAACA	TGAGAATGCTATACGGGT	300
SAHH	GGGCGGTGACCTTACTAACCTCAT	TCGAAGACAGTCCTAGGCT	300
GCSl	TCTGCCCAATTGTTATGGCTTT	GTCTGACACGTAGCCTCGGTAA	300
GCSm	GCACAGGTAAAACCCAATAGTAATCAA	CAGTCAAATCTGGTGGCATCA	300
GNMT	GGCACAGGAGTGGACTCGAT	ATCCACACTCGTGACGCTAAAG	300
18S	CCAGTAAGTGCGGGTCATAAGC	CCGATTGGATGGTTTAGTGAGG	100

*concentrations used in PCR reactions